

The convergent xenogeneic silencer MucR predisposes α -proteobacteria to integrate AT-rich symbiosis genes

Wen-Tao Shi^{1,2}, Biliang Zhang^{1,2}, Meng-Lin Li^{1,2}, Ke-Han Liu^{1,2}, Jian Jiao^{1,2,*} and Chang-Fu Tian^{1,2,*} [†]

¹State Key Laboratory of Agrobiotechnology, and College of Biological Sciences, China Agricultural University, Beijing, China and ²MOA Key Laboratory of Soil Microbiology, and Rhizobium Research Center, China Agricultural University, Beijing, China

Received December 03, 2021; Revised July 11, 2022; Editorial Decision July 12, 2022; Accepted July 21, 2022

ABSTRACT

Bacterial adaptation is largely shaped by horizontal gene transfer, xenogeneic silencing mediated by lineage-specific DNA bridgers (H-NS, Lsr2, MvaT and Rok), and various anti-silencing mechanisms. No xenogeneic silencing DNA bridger is known for α -proteobacteria, from which mitochondria evolved. By investigating α -proteobacterium *Sinorhizobium fredii*, a facultative legume microsymbiont, here we report the conserved zinc-finger bearing MucR as a novel xenogeneic silencing DNA bridger. Self-association mediated by its N-terminal domain (NTD) is required for DNA–MucR–DNA bridging complex formation, maximizing MucR stability, transcriptional silencing, and efficient symbiosis in legume nodules. Essential roles of NTD, CTD (C-terminal DNA-binding domain), or full-length MucR in symbiosis can be replaced by non-homologous NTD, CTD, or full-length protein of H-NS from γ -proteobacterium *Escherichia coli*, while NTD rather than CTD of Lsr2 from Gram-positive *Mycobacterium tuberculosis* can replace the corresponding domain of MucR in symbiosis. Chromatin immunoprecipitation sequencing reveals similar recruitment profiles of H-NS, MucR and various functional chimeric xenogeneic silencers across the multipartite genome of *S. fredii*, i.e. preferring AT-rich genomic islands and symbiosis plasmid with key symbiosis genes as shared targets. Collectively, the convergently evolved DNA bridger MucR predisposed α -proteobacteria to integrate AT-rich foreign DNA including symbiosis genes, horizontal transfer of which is strongly selected in nature.

INTRODUCTION

The prevailing symbiogenic theory of eukaryogenesis involves the symbiosis between a facultative α -proteobacterium and an archaeal host (1,2). This putative α -proteobacterium evolved into the present-day mitochondria with probably 3000–4000 genes transferred into the nucleus (3). Many mitochondria within a single eukaryote cell produce more ATP per gene than prokaryotes and contribute to the development of multicellularity and genome expansion of eukaryotes (4). On the other hand, the archaeal host provided the complex information processing machinery including histones which compacted the ever-growing eukaryotic genome, the majority of which is mobile or ‘selfish’ DNA (4,5). Despite extensive horizontal gene transfer (HGT) between prokaryotes in microbiota of various niches (6), it has been proposed that prokaryote genome size is limited by the ability to manipulate and control gene expression rather than the cost of synthesizing DNA (5). Without histone proteins, the organization of bacterial DNA depends on nucleoid-associated proteins (NAPs) involved in bending and looping of DNA (7). Known bacterial DNA bending factors are Fis (factor for inversion stimulation), IHF (integration host factor), and HU (histone-like protein from *Escherichia coli* strain U93) (7,8). DNA looping in bacteria is actively mediated by the conserved SMC (structural maintenance of chromosomes) complexes driven by ATP (9), and passively by lineage-specific DNA bridgers including H-NS (histone-like nucleoid structuring protein) (10), MvaT (11,12), Lsr2 (13,14) and Rok (15,16) reported in *Enterobacteriaceae* (Gram-), *Pseudomonas* (Gram-), *Actinomycetes* (Gram+) and *Bacillus* (Gram+), respectively. Despite low sequence homology between these lineage-specific DNA bridgers, they share convergent features such as self-association mainly mediated by their N-terminal

*To whom correspondence should be addressed. Tel: +86 10 62734009; Email: cftian@cau.edu.cn
Correspondence may also be addressed to Jian Jiao. Tel: +86 10 62734009; Email: jiaojian@cau.edu.cn
[†]Lead contact.

domain (NTD), and xenogeneic silencing function mediated by the DNA binding preference of C-terminal domain (CTD) to AT-rich foreign DNA sequences (7,17–19). However, it remains elusive whether DNA bridger(s) of such convergent features also evolved in α -proteobacteria which are enriched with symbiotic and pathogenic bacteria facultatively associated with various eukaryotes (20,21).

In 1980s, *ros* and *mucR* mutants forming rough outer surface colonies were independently identified for the plant pathogen *Agrobacterium tumefaciens* and legume nodule microsymbiont *Sinorhizobium meliloti*, respectively (22,23). MucR and Ros, or named as RosR or M1 in other species, were later demonstrated as homologs belonging to the Cys₂His₂ zinc-finger bearing MucR/Ros (PF05443) family (24–27). Evolutionary analysis further suggested a possible ancestral origin of MucR/Ros in α -proteobacteria and δ -proteobacteria, followed by multiple independent HGT and gene loss events in the evolution of the tree of life (20). The MucR/Ros family proteins have received intensive studies in plant and human pathogens (*Agrobacterium* and *Brucella*), legume microsymbionts (*Sinorhizobium*, *Rhizobium* and *Mesorhizobium*), and also in the cell cycle model *Caulobacter* (20). MucR/Ros functions as a pleiotropic transcriptional regulator for cellular processes such as biosynthesis of various exopolysaccharides (28–30), cell cycle (31), c-di-GMP signaling (32), motility and quorum sensing (33–37), secretion systems including T1SS, T3SS and T4SS (38,39), some of which are involved in virulence (40–45) and symbiosis (25,32,33,38,46–48). A combined ChIP-seq (Chromatin immunoprecipitation sequencing) and RNA-seq analysis of *Sinorhizobium fredii* revealed that MucR mainly acts as a silencer for AT-rich foreign genes with predisposed high transcription potential (38). This feature of MucR is similar to non-homologous xenogeneic silencers H-NS, Lsr2, MvaT and Rok from other bacterial classes (17,20), i.e. banking genes with potential benefits while reducing energy cost and toxicity due to random transcription of AT-rich foreign DNA (32,38,49,50).

Extensive studies of the Cys₂His₂ zinc-finger bearing CTD of MucR/Ros (such as the region 56–142 of Ros from *Agrobacterium tumefaciens*) have led to a hypothesis that the Cys₂His₂ zinc-finger structure of MucR/Ros can be the ancestral form of eukaryotic Cys₂His₂ zinc-finger (27,51–54). The single CTD of MucR/Ros can bind target DNA *in vitro* (27,55). Several cases of DNA binding by single zinc-finger domain proteins from eukaryotes also have been reported (56,57), while in most cases, a minimum of two zinc-fingers is required for high-affinity DNA binding and a protein harboring tandemly repeated zinc-fingers (as many as 37) is common in eukaryotes (54,55,58). Recently, it was found that NTD is essential for *in vitro* self-association of MucR homologs from *Mesorhizobium loti* and *Brucella abortus*, resulting in high-order oligomerization of MucR (59,60). These cumulative evidences support a hypothesis that the zinc-finger bearing MucR/Ros family protein is a novel xenogeneic silencer conserved in α -proteobacteria (20,38,59–61), though the significance of NTD mediated self-association in shaping MucR-DNA complex remains unexplored (20,59). Does MucR bridge DNA in α -proteobacteria as other lineage-specific xeno-

genic silencers? Could MucR in α -proteobacteria be replaced by non-homologous xenogeneic silencers from other bacterial classes?

In this work, we focused on MucR from the broad-host-range *S. fredii* CCBAU45436 (SF45436) associated with diverse legumes including important crops such as soybean and pigeonpea (62,63), which is essential for effective symbiosis of SF45436 (32,38,46,47). We systematically investigated the key residues and conserved sequence signatures essential for function of NTD, and the regulatory role of self-association mediated by NTD during MucR-DNA interaction. It was revealed that the Cys₂His₂ zinc-finger bearing MucR is a novel DNA bridger conserved in α -proteobacteria, with its NTD as the key modulation domain. The ability of NTD, CTD, or full-length protein of xenogeneic silencers from *E. coli* (Gram-) and *Mycobacterium tuberculosis* (Gram+) to replace corresponding non-homologous regions or full-length protein of MucR was investigated by testing symbiotic efficiency and genome-wide ChIP-seq profiles of related SF45436 derivatives. The significance of the convergently evolved zinc-finger DNA bridger MucR was further discussed in the context of bacterial pangenome evolution and adaptation.

MATERIALS AND METHODS

Strains, plasmids and growth conditions

The strains and plasmids used in this study are listed in Supplementary Table S1. *S. fredii* strains were grown at 28°C in TY medium (5 g tryptone, 3 g yeast extract, 0.6 g CaCl₂ per liter). *E. coli* strains were grown at 37°C in Luria-Bertani (LB) medium. Antibiotics were supplemented as required at the following concentrations (μ g/ml): nalidixic acid (Na), 30; gentamicin (Gen), 30; ampicillin (Amp), 100; kanamycin (Kan), 50. To test the colony phenotype, rhizobial cells pre-cultured for 48 h in TY medium were collected and resuspended in physiological saline to OD₆₀₀ = 0.2 after twice of wash. 10 μ l of each rhizobial suspension was spotted onto the agar plates of MOPS-buffered minimal medium (64) supplemented with or without Congo Red. Plates were incubated at 28°C for 3 days before taking pictures. For *E. coli* strains, cells were cultured in LB medium for 12 h to stationary phase. The bacterial suspension was collected, washed twice with physiological saline, and resuspended to OD₆₀₀ = 0.2. The serially diluted bacterial suspension (10 μ l) was spotted on LB agar plates. Colony morphology was photographed after culturing at 37°C for 24 h.

Yeast-two-hybrid assay

The coding sequences of MucR1, MucR2, different fragments of MucR1 and MucR1_{NTD} carrying various mutations were amplified by high fidelity PCR and cloned into the pGADT7 (AD) and/or pGBKT7 (BD). The desired point mutations were firstly generated on the pTOPO (T-vector, GenStar) derivative carrying the wild-type MucR1 coding sequence by site-directed mutagenesis using high fidelity circular PCR. The derived plasmids were further used as PCR templates for amplification. After validation by PCR and Sanger sequencing, the various pGADT7

and pGBKT7 plasmids were co-transformed into *Saccharomyces cerevisiae* AH109 competent cells. The yeast-two-hybrid assay was performed according to the manual of Matchmaker GAL4 two-hybrid system 3 (TAKARA). Briefly, the co-transformed yeast colony was screened on synthetically defined medium lacking Trp/Leu (SD/-Trp/-Leu). The obtained yeast single colony was resuspended in physiological saline to $OD_{600} = 0.2$. The serially diluted yeast suspension was spotted on the SD/-Trp/-Leu agar plate and SD/-Trp/-Leu/-His/X- α -Gal agar plate (containing 6.7 g/l yeast nitrogen base without amino acids, 20 g/l glucose, 1.17 g/l Dropout Supplement-Trp-Leu-His, 40 mg/l X- α -Gal, 15 g/l agar, pH5.8), and cultured at 28°C for 72 h before recording. Reagents used in SD medium were purchased from Coolaber (Beijing). The colony growth and blue color on the SD/-Trp/-Leu/-His/X- α -Gal agar plate indicate protein interaction. pGADT7-T (SV40) and pGBKT7-53 (p53) were used as positive control pair, and pGADT7-T (SV40) and pGBKT7-Lam (Lam) were used as negative control pair in the yeast-two-hybrid assay.

Genetic procedures

The primers used are listed in Supplementary Table S2. All plasmid constructs were transformed into *E. coli* DH5 α and verified by Sanger sequencing before conjugation into rhizobia via triparental mating with pRK2013 as the helper plasmid. To construct the $\Delta mucR1\&2$ double mutant, upstream and downstream ~500-bp flanking regions of *mucR2* gene were amplified and assembled with the linearized allelic exchange vector pJQ200SK (65). The derived plasmid was introduced into the $\Delta mucR1$ mutant without gentamicin resistance constructed previously (32). Single-crossover clones were screened on TY-agar plates with gentamicin and subject to passage cultivation in TY medium without any antibiotics. The double deletion mutant clones were further selected on TY-agar plates with 5% sucrose and verified by PCR and Sanger sequencing. Construction of $\Delta mucR1\&2$ mutant derivatives carrying MucR1-FLAG, Lsr2₍₁₋₅₀₎-MucR1_{CTD}-FLAG, Lsr2₍₁₋₆₅₎-MucR1_{CTD}-FLAG, MucR1_{NTD}-Lsr2₍₇₄₋₁₁₂₎-FLAG, H-NS₍₁₋₈₉₎-MucR1_{CTD}-FLAG, MucR1_{NTD}-H-NS₍₇₇₋₁₃₇₎-FLAG and H-NS-FLAG were also achieved by using allelic exchange strategy. The corresponding coding sequences of these FLAG-tagged proteins were amplified using SF45436 genomic DNA, pTOPO derivatives and chemically synthesized DNA as templates. These fragments, together with the upstream and downstream regions of *mucR1* were tandemly cloned into pJQ200SK. The pJQ200SK derivatives were conjugated into the $\Delta mucR1\&2$ double mutant for screening single-crossover and double-crossover clones. Finally, pJQ200SK mediated allelic exchange strategy introduced a single copy gene into the genome. For the plasmids used for complementing the Δhns mutant of *E. coli* (66), the promoter of *hns* (300 bp), the coding sequences of H-NS-FLAG, Lsr2-FLAG, MucR1-FLAG, Lsr2₍₁₋₆₅₎-MucR1_{CTD}-FLAG, MucR1_{NTD}-Lsr2₍₅₁₋₁₁₂₎-FLAG and MucR1_{NTD}-Lsr2₍₇₄₋₁₁₂₎-FLAG were assembled into Sma I-linearized pBBR1MCS2 and then transformed into Δhns .

Protein 3D structure modeling

All 3-dimensional models of MucR1, H-NS and chimeric proteins explored in this study were predicted by AlphaFold2_mmseqs2 server using default setting parameters and oligomer states (67,68). Alignment and visualization of models were carried out by using Open-Source PyMOL 2.1.0. Interface residues between two chains of MucR1_{NTD} dimer were identified by running InterfaceResidues.py script from PyMOLWiki (<https://pymolwiki.org>).

Plant assay

Symbiotic performance of *S. fredii* strains was tested on *Glycine soja* WSD (62). Seeds were surface-sterilized in 3% NaClO (wt/vol) solution after treatment with concentrated sulfuric acid for 10 min and germinated for 36–48 h under dark condition. Seedlings were then sown into vermiculite moistened with low-N nutrient solution in Leonard jars and inoculated with 1 mL physiological saline suspension of rhizobia with $OD_{600} = 0.2$. Plants were grown at 24°C with a 16-h illumination period for 28 days. Leaf chlorophyll content was measured by a SPAD-502 Meter (Konica Minolta) as described previously (63). Two independent experiments were carried out.

Western blotting

To monitor the protein levels of MucR1 and its derivatives at different growth phases, rhizobial cells cultured in TY medium were sampled every 3 h in a time-course manner that started from $OD_{600} \approx 0.3$. The cell pellets were resuspended in corresponding volume of SDS-loading buffer to normalize the cell density and then lysed by boiling for 10 min. The lysates were separated on 12% SDS-PAGE and transferred to nitrocellulose membranes. For immunodetection of individual proteins, mouse monoclonal anti-FLAG M2 antibody (Sigma), HRP (horseradish peroxidase)-conjugated Goat Anti-Mouse IgG (Abcam), and eECL Western Blot Kit (CW BIO) were used and chemiluminescence signals were captured and quantified using a Fusion FX6 (Vilber) and the Evolution-Capt Edge software.

Protein stability assay

To detect the protein stability of MucR1 and MucR1_{Y24G} under *in vivo* conditions, the promoter of *mucR1* (486 bp) and coding sequences of these two proteins and C-terminal fused FLAG-tag were tandemly cloned into pBBR1MCS-2. The $\Delta mucR1$ mutant derivatives carrying pBR-MucR1-FLAG and pBR-MucR1_{Y24G}-FLAG were cultured in TY medium until $OD_{600} = 0.8$. Cells were pelleted and resuspended in PBS supplemented with 50 μ g/ml chloramphenicol. After treatment with indicated time, samples were stopped by adding 5 \times SDS-loading buffer and boiling for 10 min. The lysates were separated in 12% SDS-PAGE and further analyzed by western blotting.

RNA extraction and RT-qPCR

Bacterial cell cultures were collected in a time-course manner as indicated, and the cell pellets were stored at -80°C before use. The bacterial total RNA kit (ZOMANBIO) was used for total RNA extraction from frozen cell pellet samples. The integrity of the resulting RNA samples was validated by agarose gel electrophoresis. RNA sample concentration and purity were measured by NanoPhotometer™ (Implen). Only qualified RNA samples were used for subsequent experiments. cDNA was synthesized from 500 ng RNA samples by using FastKing-RT SuperMix (TIANGEN). The resulting cDNA was diluted 500 times and used as the template for subsequent quantitative PCR. Reverse transcription quantitative PCR was performed with gene-specific primers using RealStar Green Fast Mixture (Genstar) and a QuantStudio™ 6 Flex Real-Time PCR System (Thermal Fisher Scientific; pre-denature stage, 95°C , 10 min; PCR stage, denature, 95°C , 15 s; anneal and elongate, 60°C , 1 min; 40 cycles). The 16S rRNA gene was used as internal reference to normalize the expression level of the wild-type and mutated *mucR1* genes. The specificity and reliability of primers were assessed by melting curves and Sanger sequencing of RT-qPCR products. Algorithm $2^{-\Delta\text{Cq}}$ was used to quantify the target gene's transcription level relative to the 16S rRNA gene. Three independent experiments were performed.

Protein purification

E. coli BL21(DE3) carrying pET30a-SUMO derivatives harboring His₆-SUMO-MucR1, His₆-SUMO-MucR1_{Y24G}, His₆-SUMO-MucR1-FLAG or His₆-SUMO-MucR1_{Y24G}-FLAG was cultured in 500 ml LB medium until $\text{OD}_{600} = 0.8$. Then IPTG was supplied to a final concentration of 0.6 mM in these cultures which were then cultured at 18°C , 150 rpm for 12 h. Cells were harvested by centrifugation (5000 g, 5 min, 4°C) and resuspended in 30 ml lysis buffer (25 mM Tris, pH8.0, 250 mM NaCl, 10 mM imidazole) supplemented with 0.1 mg/ml DNase I, 0.4 mg/ml lysozyme and protease-inhibitor cocktail (Roche). After 30 min of incubation and 120 cycles of sonication (300 W, 10 s on, 10 s off) on ice, the lysate was cleared by centrifugation (18 000 g, 4°C , 30 min) and filtration through a 0.22 μm membrane. The supernatant was loaded onto lysis buffer pre-washed Ni-Agarose Resin (CW-BIO), and washed three times with wash buffer (lysis buffer with 20/50 mM imidazole) and then eluted with imidazole gradient elution (lysis buffer with 100, 200, 300 mM imidazole). The purified proteins were concentrated by ultrafiltration and redissolved in storage buffer (25 mM Tris, pH 8.0, 250 mM NaCl, 10% glycerol) before use or storage at -80°C . Due to the strong hydrophobicity of MucR1_{NTD}, it is difficult to obtain high concentration of soluble His₆-MucR1 protein. To avoid potential influence of His₆-SUMO tag on the subsequent experiments, HRV-3C protease was used to cleave His₆-SUMO tag before *in vitro* protein cross-linking assay where 0.021 μM protein was sufficient. By contrast, for electrophoretic mobility shift assay (EMSA) and DNA-bridging assay which need high concentration of MucR1 and MucR1_{Y24G} proteins in the gradient (from

0.5 μM to 64 μM), the N-terminal His₆-SUMO tag was cleaved by HRV-3C protease after incubation of DNA with His₆-SUMO-MucR1 or His₆-SUMO-MucR1_{Y24G} to avoid protein precipitation as described previously (32).

In vivo and *in vitro* protein cross-linking assay

For *in vivo* protein cross-linking assay, 50 mL TY culture ($\text{OD}_{600} = 1.2$) of each *S. fredii* strains was pelleted by centrifugation (5000 g, 5 min, 4°C) with twice wash in pre-cooled PBS. Each cell pellet was resuspended in 12 ml PBS supplemented with 10 μl EDTA-free protease-inhibitor cocktail (Roche), 0.1 mg/ml DNase I and 0.4 mg/ml lysozyme, and incubated on ice for 30 min. 50 μl lysates were transferred to new tubes as the control sample. Glutaraldehyde was added to the lysates at a final concentration of 0.02% and incubated on ice for 15 min. 50 μl of cross-linking sample was pipetted and quenched by adding 10 μl 1 M Tris (pH8.0). For *in vitro* protein cross-linking assay, the purified His₆-SUMO-MucR1-FLAG and His₆-SUMO-MucR1_{Y24G}-FLAG were diluted to 10 $\mu\text{g}/\text{ml}$ in PBS containing 1 mM dithiothreitol and were then digested with HRV-3C protease to cleave the N-terminal His₆-SUMO tag. The cleaved proteins were further dialyzed in PBS (pH7.4) and incubated with Ni-Agarose Resin (CW-BIO) to remove dithiothreitol, His₆-SUMO and noncleaved proteins. The MucR1-FLAG and MucR1_{Y24G}-FLAG samples were normalized to 0.021 μM (0.4 $\mu\text{g}/\text{ml}$). Cross-linking reactions were conducted on ice for 8 min or 16 min in the presence of 0.02% glutaraldehyde under conditions with or without various concentrations of DNA probes: the 228-bp *Puxs1*, the 1069-bp probe harboring this 228-bp region, and the pTOPO-1069 carrying this 1069-bp region. The samples were separated in 12% SDS-PAGE and further analyzed by western blotting.

Electrophoretic mobility shift assay (EMSA)

The electrophoretic mobility shift assay was performed as previously described (32), with modifications as follows. DNA probes were prepared by PCR amplification with the pTOPO plasmid carrying corresponding intergenic regions as templates or annealing complementary synthesized DNA strands using 5'-Cy5-labeled and unlabeled primers as listed in Supplementary Table S2. The binding reaction mixture (10 μl) consisted of 1 mg/ml bovine serum albumin, 1 mg/ml sonicated salmon sperm DNA, 1, 10 or 12.3 nM Cy5-labeled DNA probe, and test proteins in the Tris-KCl buffer (25 mM Tris (pH8.0), 100 mM KCl, 5% glycerol, 0.05% dodecyl- β -D-maltopyranoside) or the PBS buffer (pH 7.4). The samples were incubated at 25°C for 30 min. Next, 1 μl HRV-3C protease (200 ng/ μl ; 10 mM dithiothreitol) was added and incubated for 30 min to cleave the N-terminal His₆-SUMO tag. To test whether MucR1 can bind to the minor or major groove of DNA, the reagents netropsin and methyl green that specifically bind to the minor and major groove of DNA, respectively, were added as indicated (69,70). The samples were separated in a 6% TB polyacrylamide gel (no EDTA), and the gel was scanned with an Azure Biosystems.

DNA-bridging assay

DNA-bridging assay was performed by using the method described previously (71), with modifications as follows. The DNA probes were prepared by PCR amplification using 5'-Cy5 or 5'-biotin labeled primers as listed in Supplementary Table S2. For each bridging assay, 100 μ l hydrophilic streptavidin magnetic beads (NEB) were washed twice with 500 μ l PBS and then resuspended in 500 μ l coupling buffer (20 mM Tris-HCl, pH7.4, 1 mM EDTA, 500 mM NaCl). Next, 10 pmol biotin-labeled DNA was added into the suspension and incubated with the beads for 30 min at room temperature with gentle rotation. After incubation, the beads were washed twice with 500 μ l incubation buffer (20 mM Tris, pH 7.4, 150 mM NaCl, 1 mM dithiothreitol, 5% glycerol (vol/vol), 0.05% Tween 20) and resuspended in incubation buffer supplemented with 10 pmol Cy5-labeled DNA and 10 μ l HRV-3C protease to a final volume of 500 μ l. The beads suspension was then divided into 50 μ l aliquots. Two-fold serially diluted protein samples were added into each of the 50 μ l aliquots and supplemented with incubation buffer to a final volume of 60 μ l. After a 30 min incubation at room temperature with gentle rotation, the mixture was placed on a magnetic stand for 5 min. The supernatant was transferred into a new tube and marked as sample *A*. 60 μ l elution buffer (incubation buffer supplemented with 0.1% SDS and 20 μ g/ml biotin) was added to the beads and incubated in boiling water for 10 min. The eluted sample was transferred into a new tube and marked as sample *B*. The Cy5 fluorescence signals of sample *A* and sample *B* were detected by a Microscale Thermophoresis Monolith NT.115 system (NanoTemper). The Cy5 fluorescence signal of sample *A* from the reaction without adding protein was defined as 100% input signal. The sample *A* was also subject to EMSA to check the relative amount of free DNA probe and that bound by MucR1 or MucR1_{Y24G}.

Chromatin immunoprecipitation sequencing (ChIP-seq) and ChIP-qPCR

S. fredii strains expressing MucR1, H-NS, or chimeric proteins with C-terminal FLAG were cultured in TY medium until OD₆₀₀ = 1.2. Formaldehyde was added to the culture to a final concentration of 1%. Cross-linking reactions were sustained for 15 min at 28°C with 180 rpm shaking, and quenched for 15 min after adding glycine to a final concentration of 100 mM. The cross-linked cells were harvested (5000 g, 5 min, 4°C) and washed twice with pre-cooled PBS. The cell pellets were ground into fine powder in liquid nitrogen and resuspended in ChIP buffer (50 mM Tris, pH8.0, 150 mM NaCl, 5 mM EDTA, 0.1% deoxycholate sodium, 1% Triton X-100). Cell lysates were sonicated to shear DNA fragments to an average length of 300–400 bp in a bath sonicator (Q800R3, QSonica) and cleared by centrifugation (13 000 g, 20 min, 4°C). For each ChIP reaction, the supernatant containing 4 mg protein was pre-cleared by 10 μ l Dynabeads M-280 (Invitrogen) and then mixed with 5 μ l anti-FLAG M2 antibody (Sigma) overnight at 4°C with gentle rotation. 50 μ l of beads were added to the samples and incubated at 4°C for 4 h with gentle rotation. The beads were washed twice with ChIP buffer, and once

with high salt buffer (50 mM Tris, pH 8.0, 500 mM NaCl, 5 mM EDTA, 0.1% deoxycholate sodium, 1% Triton X-100), LiCl wash buffer (10 mM Tris, pH8.0, 250 mM LiCl, 0.05% deoxycholate sodium, 1 mM EDTA) and TE buffer (10 mM Tris, pH 8.0, 1 mM EDTA). The protein-DNA complex was eluted in 500 μ l elution buffer (1% SDS, 0.1 M NaHCO₃). To reverse the cross-linking, the eluted samples were supplemented with NaCl to a final concentration of 300 mM, incubated overnight at 65°C and further digested by 0.5 mg proteinase K for 2 h at 45°C. ChIP DNA was extracted using phenol:chloroform:isoamylalcohol (25:24:1), ethanol precipitated using Dr GenTLE Precipitation Carrier (TAKARA). 100 μ l of the pre-cleared supernatant was used for total chromatin input DNA preparation. The recruitment level of FLAG-tagged proteins in *PmucR1* and *Puxs1* was detected by ChIP-qPCR to assess the quality of ChIP DNA. The total chromatin input DNA was diluted to 1 ng/ μ l, and the ChIP DNA was diluted 250 times. These diluted DNA samples were used as the template for subsequent qPCR. An 80-bp fragment inside SF456436_b52410 with no protein recruitment signal was amplified by the primers ngtv-QF/ngtv-QR and used as an internal reference to normalize protein recruitment levels in *PmucR1* and *Puxs1*. Subsequent qPCR was performed as described in RT-qPCR. Algorithm $2^{-\Delta\Delta C_q}$ was used to quantify protein recruitment levels. The primers used are listed in Supplementary Table S2. Library construction and deep sequencing (paired-end 150 using HiSeq 3000; Illumina) were performed by Novogene-Beijing, with the total chromatin input DNA as control. Three biological replicates were tested. ChIP-seq reads mapping, peak calling, peakID unification between samples and target gene association were performed as previously described (38).

Hemolytic activity assay

The hemolytic activity was detected as previously described with minor modifications (13). In brief, two independent colonies per strain were stabbed into the blood agar plates containing 3% tryptic soy powder, 1.5% agar and 5% defibrinated sheep blood (Solarbio) and incubated at 37°C for 24 h before recording. A clear zone around the *E. coli* colony indicated hemolytic activity caused by the lysis of red blood cells.

RESULTS AND DISCUSSION

The N-terminal domain is essential for self-association and stability of MucR1

The number of MucR copies within a genome ranges from 1 to 45 in α -proteobacteria and 1 to 6 in δ -proteobacteria, showing multiple independent duplication and horizontal transfer events (20). *S. fredii* CCBAU45436 (SF45436) has two MucR copies, with MucR1 as a functional xenogeneic silencer of pleiotropic regulatory roles while MucR2 being unable to bind DNA due to a frame shift mutation in its C-terminal DNA binding domain (32,38,46) (Figure 1A). The CTD of MucR/Ros alone can bind DNA *in vitro* (27) and its NMR structure (PDB: 2jsp for Ros87 from *A. tumefaciens*) showed RMSD (root-mean-square deviation) values of 1.263 Å and 1.099 Å, respectively, com-

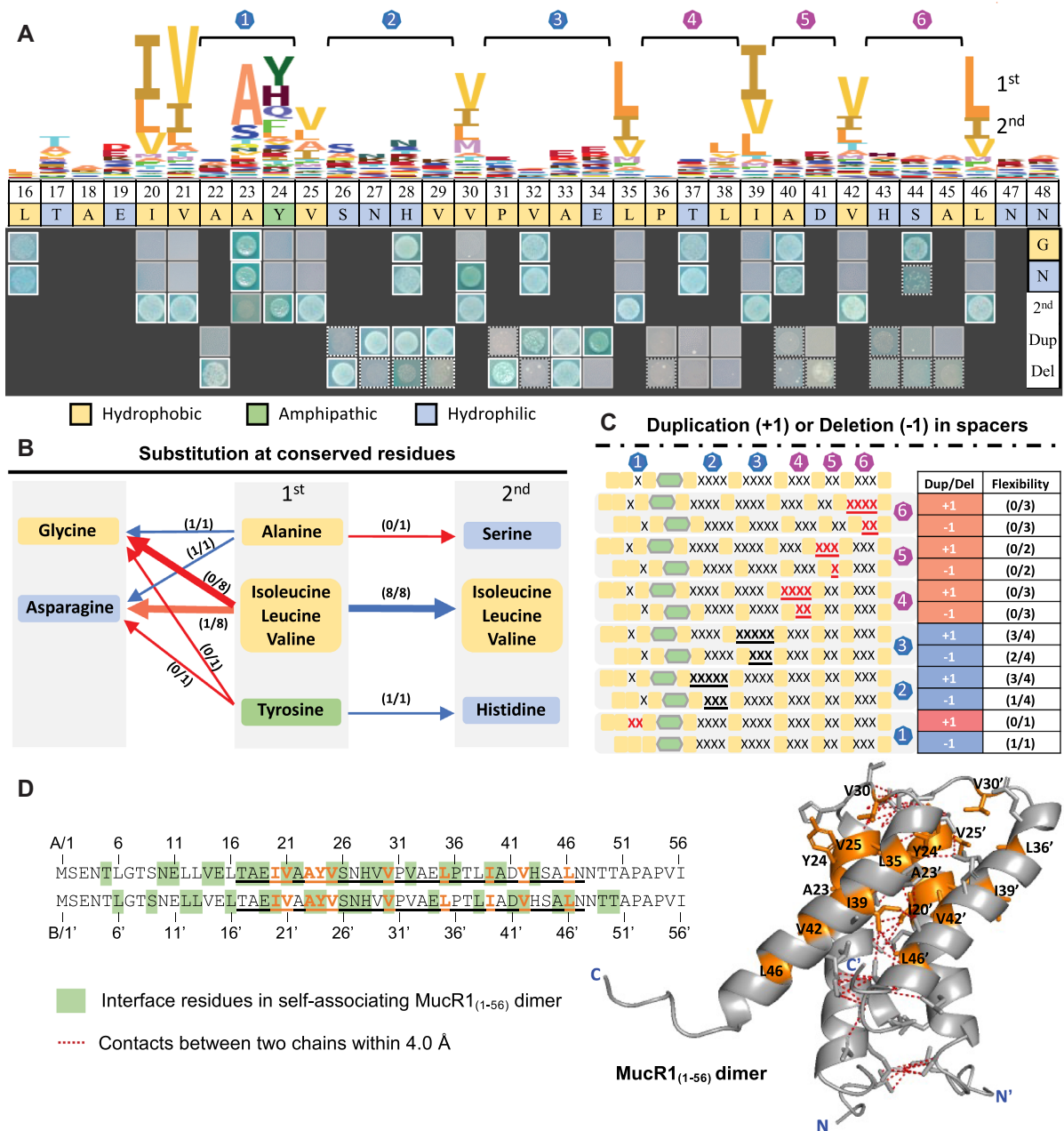


Figure 2. Identification of key residues and their spacers in NTD involved in self-association. (A) The yeast-two-hybrid assay of MucR1₍₁₋₅₆₎ derivatives (the same fragments were cloned in AD and BD). The HMM logo is based on 2201 MucR/Ros homologs in the Pfam database (871 species). The key residues (1st) were substituted by G, N or the secondly conserved residue (2nd). ‘Dup’, duplication; ‘Del’, deletion. Six spacers between conserved branched-chain Ile/Val/Leu are indicated by blue and purple numbers. (B) Summary for proteins with substitutions at conserved residues. Red and blue arrows represent loss and maintenance of self-association ability, respectively. (C) Summary for proteins with duplication (+1) or deletion (-1) of the same residue ‘X’ in spacers. (B, C) The numbers in brackets (x/y) indicate x out of y test proteins maintained self-association ability. (A–C) Hydrophobic, amphipathic, and hydrophilic residues are indicated in different colors. (D) MucR1_{NTD} dimer predicted by AlphaFold2. Orange, conserved residues. Side chains of conserved residues and/or interface residues ($\Delta\text{ASA} > 1.0$) are shown in stick mode. ΔASA , changes in accessible surface area.

tion (-1) of representative spacer residues were constructed and tested for the self-association ability in the yeast-two-hybrid assay (Figure 2A and C). It turned out that the length of spacers within the L35–I39–V42–L46 fragment was under strong natural selection (spacer ID: 4, 5, and 6; Figure 2C) while those within the V21–V25–V30–L35 region showed flexibility to certain extent (spacer ID: 1, 2 and 3; Figure 2C). Within the V21–V25 spacer (ID: 1), hydropho-

phobic A23 can be substituted by Gly or Asn without defects in self-association whereas substitution by the second abundant S23 had a notable defect (Figure 2A and B), implying potential context effect of surrounding residues. In addition to these conserved hydrophobic residues, the 24th residue of MucR homologs is distinct for its most abundant amphipathic Tyr carrying a -N-H group on its aromatic ring or the second abundant His harboring two titratable -

N–H groups (Figure 2A). The Y24 of MucR1_(1–56) can be substituted by the second abundant H24 but not by non-polar Gly or neutral polar Asn (Figure 2A and B). It has been shown that the number of His-containing networks on the subunit surface of a protein together with the strength of surrounding hydrophobic interactions allow pH-driven conformational changes of helical bundles, and this process is mediated by the pH responsive His protonation levels and hydrogen-bond networks (75). Moreover, π – π stacking and hydrogen-bonding interactions mediated by aromatic moieties of Tyr pairs facilitate the interaction between neighboring α helix (76). Therefore, despite a considerable divergence in NTD among 2201 MucR homologs (Figure 2A), key residues and their spacer length have been under strong natural selection to ensure self-association as also indicated in the MucR1_(1–56) dimer predicted by AlphaFold2 (Figure 2D).

To test if MucR1 can self-associate *in vivo* in SF45436, the cross-linking assay was performed for the Δ *mucR1&2* double mutant carrying MucR1-FLAG or its derivatives with representative substitutions (Y24G, C82G, Y24G&C82G, V21G) or deletions (V29-, and Δ 2–56) (Figure 3A). The wild-type MucR1 can form dimer and putative higher-order oligomers *in vivo*. The MucR1_{C82G} has a substitution in the Cys₂His₂ zinc-finger motif (X₂-Cys79-X₂-Cys82-X₉-His92-X₂-His96) that is essential for DNA binding (52), and exhibited a stronger signal for monomer, dimer and putative higher-order oligomers (Figure 3A). This is in line with the evidence that MucR1 directly represses its own transcription (38). These cross-linking results were supported by docking analysis of either NTD (Figure 3B) or full-length MucR1 (Figure 3C and Supplementary Figure S1) using AlphaFold2 (68). Briefly, the NTD homo-dimer was characterized by its two sets of longitudinally arranged α helices corresponding to the region covering three spacers (ID: 4–6) under strong selection (magenta in Figure 3B), and that covering spacers showing relatively higher flexibility (ID: 2–3), respectively. The NTD homo-tetramer and homo-octamer are organized in a circle-like manner (Figure 3B). These self-association patterns mediated by α helices and the adjacent low complex linker region connecting CTD (as exemplified by tetramer in Figure 3C) may allow the MucR1 oligomers to bind multiple sites of DNA. Therefore, both *in vitro* (59–61) and *in vivo* evidences support self-association of MucR1.

Moreover, it is noteworthy that MucR1 Δ _{2–56} with a truncated NTD (lacking the 2–56 fragment) showed a low protein level under test conditions (Figure 3A). Similar results were observed for those MucR1 derivatives with substitutions at a conserved branched-chain amino acid (V21G) or at the amphipathic Y24 (Y24G and Y24G&C82G), and MucR1 with a shortened spacer in the V25–V30 region of NTD (V29-) (Figure 3A). The low protein levels of these MucR1 derivatives *in vivo*, due to either low expression levels or impaired protein stability, made it unfeasible to draw any conclusions on the role of NTD in self-association *in vivo*. To explain why protein levels of these MucR1 derivatives are low *in vivo*, protein and transcriptional levels of representative MucR1 derivatives (Y24G, Y24G&C82G, C82G) were further monitored at exponential phase and stationary phase (Figure 4A). Throughout the 12 sampling points spanning more than 30 h (Figure 4A), the protein

level of MucR1_{C82G} was higher than MucR1 which was in turn higher than MucR1_{Y24G} and MucR_{Y24G&C82G} (Figure 4B), whereas the transcriptional levels of MucR1_{Y24G} and MucR_{Y24G&C82G} were indistinguishable from MucR1_{C82G} and higher than MucR1 (Figure 4C). The high transcriptional and protein levels of MucR1_{C82G} are consistent with the essential role of zinc-finger (X₂-Cys79-X₂-Cys82-X₉-His92-X₂-His96) bearing CTD of MucR1 in transcriptional repression of *mucR1* (38,52). We further wondered if the higher transcription level of MucR1_{Y24G} compared to MucR1 was due to derepression mediated by potentially impaired DNA binding ability or/and reduced protein stability of MucR1_{Y24G}. EMSA (electrophoretic mobility shift assay) with an equal quantity of purified MucR1_{Y24G} and MucR1 (Supplementary Figure S2) showed that no discrete bandshift was observed at low protein:DNA ratios implying unstable and disintegrating protein-DNA complex (Figure 4D). Moreover, upon adding increasing amounts of protein for both MucR1 and MucR1_{Y24G} (Figure 4D), the protein-DNA complex shifted further (Figure 4D). The bandshift of the *PmucR1* probe was more significant in the presence of saturated MucR1 than with saturated MucR1_{Y24G} (Figure 4D), implying more MucR1 than MucR1_{Y24G} bound to DNA probe. These results are in line with a working model that MucR1_{Y24G} is unable to self-associate but still individually binds to multiple binding sites in the *PmucR1* probe. However, this interaction between MucR1_{Y24G} and *PmucR1* failed to repress the transcription of *mucR1* as observed in Figure 4C. On the other hand, when the *in vivo* translation process at the mid-log phase was inhibited by adding chloramphenicol (Figure 4E), MucR1_{Y24G} exhibited a fast decline in protein stability within 4 h while MucR1 was fairly stable 24 h post translation inhibition. Therefore, the NTD is essential for maintaining the maximum stability of MucR1 *in vivo*.

As revealed above, it is not feasible to investigate the role of NTD in self-association of MucR1 *in vivo* (Figure 3A), largely due to the impaired stability of MucR1 derivatives with key mutations in NTD (Figure 4E). Moreover, the potential interactions of MucR1 with other proteins might lead to a false positive signal of high-order multimers observed *in vivo* cross-linking assay (Figure 3A). Consequently, purified MucR1-FLAG and MucR1_{Y24G}-FLAG were tested in the *in vitro* cross-linking assay (Figure 5A). It is clear that MucR1-FLAG was able to self-associate in dimer and high-order oligomers while MucR1_{Y24G}-FLAG exhibited significant defects in self-association. To test if the presence of target DNA can affect the self-association process of MucR1, the promoter region of *uxs1* targeted by MucR1, revealed earlier (28,38) and confirmed herein (Supplementary Figure S3), was included in the *in vitro* cross-linking assay (Figure 5B). The amount of MucR1 dimer increased with the concentration of the *Puxs1* probe (from 0 to 5 nM; 228 bp) (Figure 5B). Similar results were obtained when 5 nM of a longer DNA probe (1069 bp) harboring the 228-bp *Puxs1* region or a plasmid-based probe carrying this 1069-bp region (pTOPO-1069; 2934 bp) (Supplementary Figure S4). In short, MucR1 self-associates mainly in the form of dimer and also in various high-order multimer forms under test conditions, which depends on its NTD and can be enhanced by target DNA.

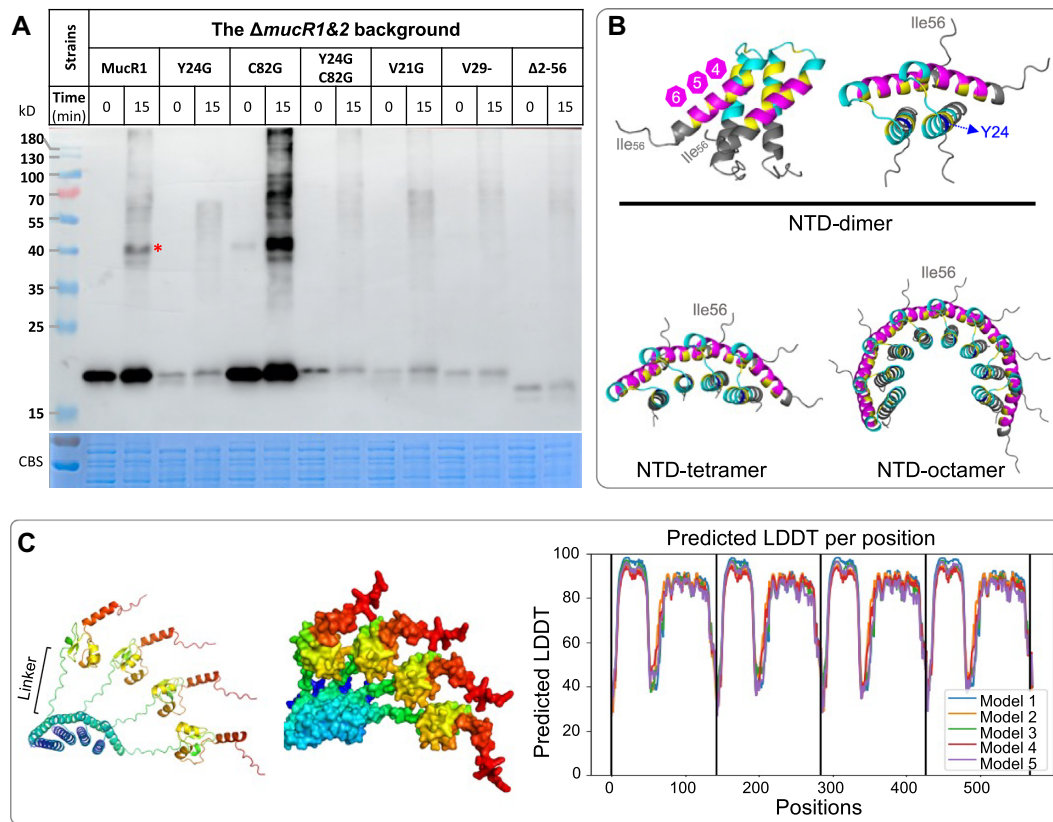


Figure 3. *In vivo* cross-linking assay of MucR1 and its derivatives, and predicted homo-multimers of MucR1. (A) Late log phase cultures ($OD_{600} = 1.2$) were subject to cross-linking by glutaraldehyde for 15 min and resolved by SDS-PAGE. The anti-FLAG antibody was used to detect MucR1 and its derivatives (substitutions and deletions). Samples were normalized by bacterial OD_{600} . *, red asterisk indicates dimer. (B, C) Predicted protein structure of homo-multimers of the NTD (B) or homo-tetramer of full MucR1 (C) by AlphaFold2. Structure for the top 1 model is shown (based on local-distance difference test; Supplementary Figure S1 for details). The color scheme in (B). Blue, Y24; yellow, conserved branched-chain residues; cyan, spacers ID1-3; magenta, spacers ID4-6. Low complex linker region is indicated in (C).

The N-terminal domain is essential for DNA-bridging ability of MucR1

It has been proposed that xenogeneic silencer H-NS from *E. coli* represses gene transcription by bridging DNA fragments (7,18). The DNA-bridging ability has also been demonstrated for the other documented lineage-specific xenogeneic silencers Lsr2 (77), MvaT (78) and Rok (79). Here we tested whether MucR1 could have this DNA-bridging ability. The notable supershift of protein-DNA complex in EMSA for the 228-bp *P_{uxs1}* probe was observed when the protein:DNA ratio was increased in the treatment of MucR1 or MucR1_{Y24G} (Supplementary Figure S3). This is similar to canonical xenogeneic silencers which extensively bind DNA in a way that additional dimers bind next to and associate with dimers or multimers already bound to the DNA (18).

Our previous ChIP-seq analysis of MucR1 uncovered the 10–11 bp periodic repeats of T or TT among MucR1 binding peaks (38), which are in line with the ‘class A flexible patterns’ TTxxxGxxxTxxxxxxxxTT (80) and an EMSA verified Ros binding motif TxxxxxGxxxxxT (81). Sequence analysis identified three TTxxxGxxxTxxxxxxxxTT motifs (named as motif_a) and ten TxxxxxGxxxxxT motifs (named as motif_b) in this *P_{uxs1}* probe (Figure 6A; mo-

tifs were sequentially numbered from right to left to reflect their relative position to the *uxs1* start codon). The ability of MucR1 to bind 12 fragments harboring these individual motifs was tested by EMSA (Supplementary Figure S5 and S6). All test fragments except those carrying motif_b10 (AT% = 31%) or motif_b9 (AT% = 15%) can be effectively bound by MucR1 at relatively low MucR1:DNA ratios. Within the *P_{uxs1}* region, four fragments (20–29 bp) covering the other regions without motif_a or motif_b can also be effectively bound by MucR1 (Supplementary Figure S7), and their AT content range from 55% to 83% (Supplementary Figure S7). These results raised a question of to what extent either motif_a or motif_b can modulate MucR1 recruitment efficiency. To answer this question, MucR1 recruitment efficiency by two representative fragments carrying motif_a.1 and motif_b.8, respectively, was compared to their corresponding random probes (without motifs but of the same nucleotide composition) and motif-substituted probes (the T/A at both ends of these putative high-affinity motifs substituted by G/C). Random probes exhibited smaller difference in MucR1 recruitment efficiency compared to wild-type probes than those motif-substituted probes did (Supplementary Figure S5). For example, in the presence of 9.28 μ M MucR1, random probes and motif-substituted probes showed $2.99 \pm 1.56\%$ and

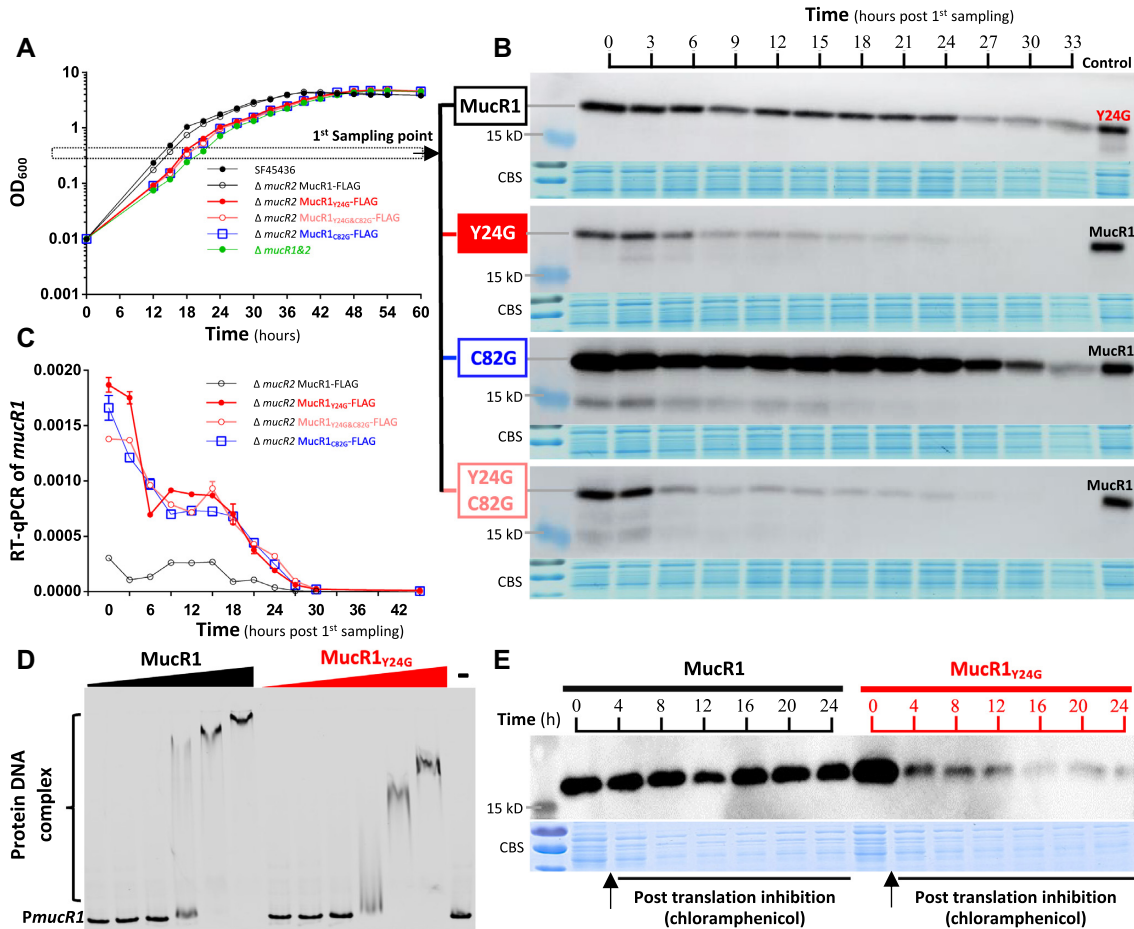


Figure 4. Post translation stability of MucR1 depends on its NTD. (A) Growth curves of test strains. (B) Dynamic protein levels of MucR1 and its derivatives. The 1st sampling point is indicated in (A). (C) Dynamic transcription levels of *mucR1* and its derivatives (relative to 16S rRNA gene). Error bars represent SD of three biological replicates. The 1st sampling is indicated in (A). (D) EMSA showing impaired bandshift of the *PmucR1* (the promoter of *mucR1*) in the treatment of MucR1_{Y24G} compared to MucR1. The *PmucR1* probe, 12.3 nM. Protein concentration: 0.5, 1.5, 4.5, 13.5, 27 and 54 μ M. ‘-’, 0 μ M. (E) Protein stability assay of MucR1 and MucR1_{Y24G} in the $\Delta mucR1$ mutant carrying pBR-MucR1-FLAG or pBR-MucR1_{Y24G}-FLAG post translation inhibition by chloramphenicol treatment of mid-log phase culture (OD₆₀₀ = 0.8).

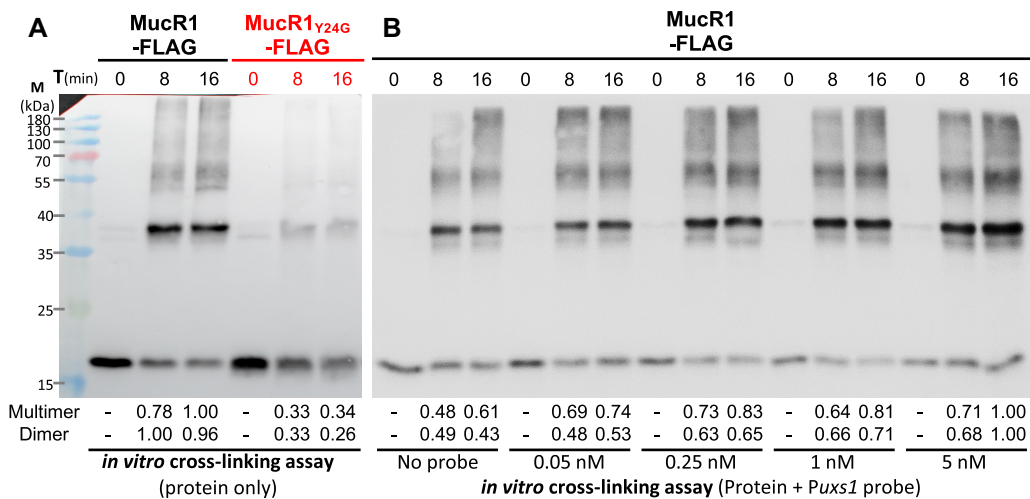


Figure 5. *In vitro* self-association of MucR1 depends on NTD and enhanced by target DNA. (A) *In vitro* cross-linking assay of MucR1-FLAG and MucR1_{Y24G}-FLAG. (B) *In vitro* cross-linking assay of MucR1-FLAG with various concentrations of DNA probe *Puxs1*. The numbers below the picture refer to the quantified band intensity values of dimers or multimers in each lane. Multimers of different oligomerization levels were collectively quantified.

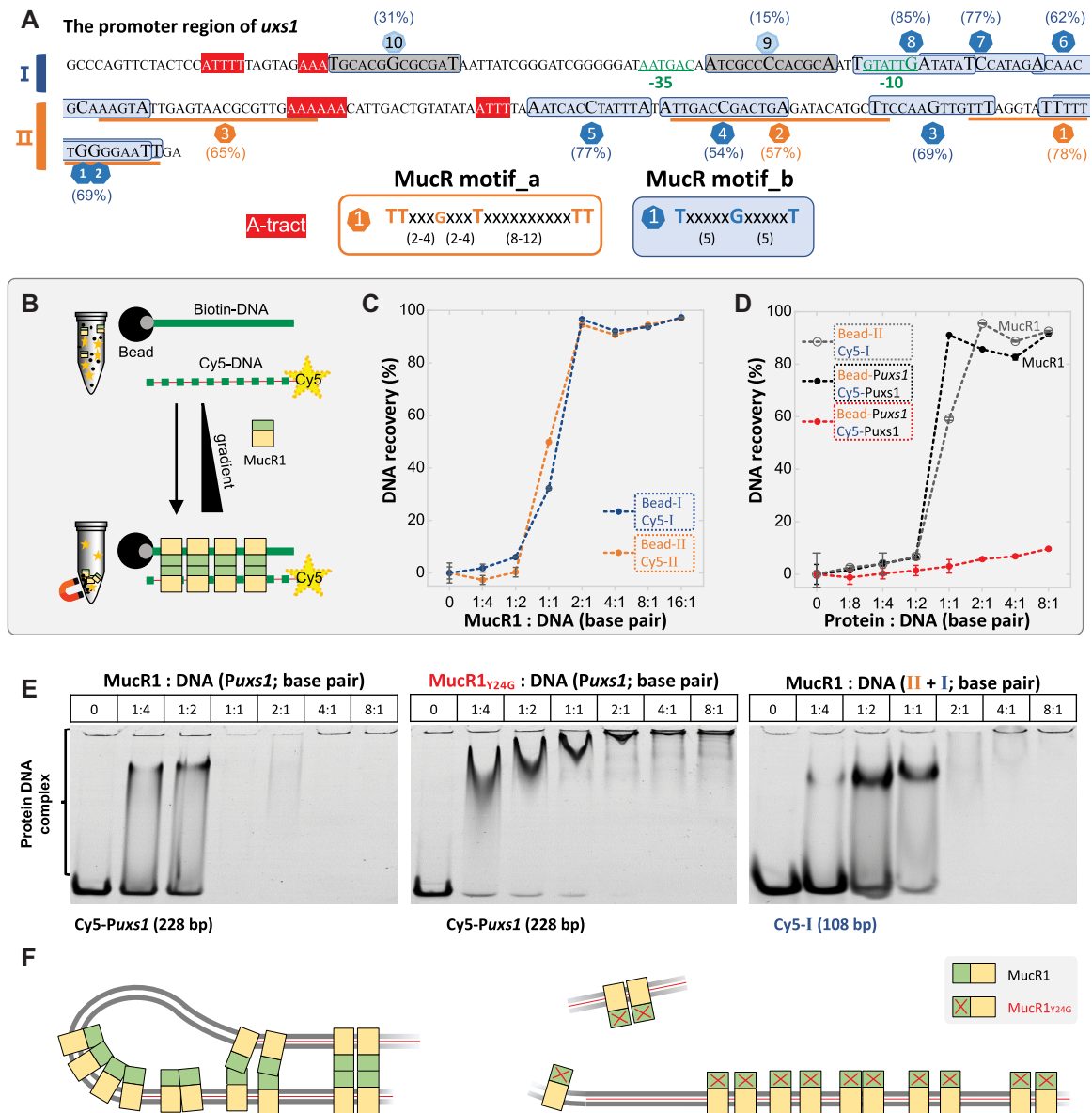


Figure 6. DNA bridging mediated by MucR1 requires a functional NTD. (A) Distribution of two putative high-affinity binding motifs (with AT content indicated in brackets) and $-10/-35$ boxes inside the *Puxs1*. The fragments I (108 bp) and II (120 bp) are indicated. EMSA for 16 fragments fully covering the 228-bp *Puxs1* is shown in Supplementary Figures S5-S7. The fragments corresponding to motif_b₁₀ and motif_b₉ show low binding affinity by MucR1 (Supplementary Figure S5-S7). (B) Schematic view of protein-DNA bridging assay. Black ball, streptavidin magnetic bead; gray-ball-labeled green solid line, biotin-labeled DNA probe; yellow-star-labeled green dashed line, Cy5-labeled DNA probe. (C) MucR1 can bridge the fragment I anchored on beads (Bead-I) and Cy5-labeled I in the supernatant (Cy5-I) (108 bp), or ‘Bead-II’ and ‘Cy5-II’. (D) MucR1 can bridge the 228-bp *Puxs1* (filled black circles), or ‘Bead-II + Cy5-I’ (open grey circles) while MucR1_{Y24G} almost loses the bridging function on the 228-bp *Puxs1* (filled red circles). Error bars represent SD of four measurements for two biological replicates from one out of two independent experiments. (E) EMSA of the supernatant sample in bridge reaction system showing the dosage dependent interactions between MucR1 or MucR1_{Y24G} and Cy5-labeled DNA probes. (F) Working model for DNA bridging mediated by MucR1 NTD (green). MucR1_{Y24G} is not able to efficiently mediate DNA bridging.

$13.27 \pm 0.02\%$ (mean \pm SD) difference, respectively, in their free probe proportion compared to their corresponding wild-type probes. A similar trend can be found when lower concentrations of MucR1 were used (Supplementary Figure S5). Although motif-substituted probes exhibited significantly lower MucR1 recruitment efficiency, these A/T to G/C substitutions did not abolish the interaction (Supplementary Figure S5). This finding was further supported by motif-substituted probes derived from the other 10 frag-

ments carrying either motif_a or motif_b (Supplementary Figure S6). Therefore, the extensive binding of MucR1 to DNA does not rely heavily on these motifs.

The observed higher MucR1 recruitment efficiency by wild-type probes carrying the 10–11 bp periodic T or TT motifs than the mutated probes with A/T substituted by G/C is more likely due to the decreased AT content. This is in line with the preference for AT-rich sequences by MucR1 and other known xenogeneic silencers (17,38). Indeed, mo-

tif_b_10 (AT% = 31%) and motif_b_9 (AT% = 15%) are of lower AT content compared to the other motifs (54–85%) (Figure 6A) and the genome average (36.9%). Among test fragments harboring motif_b of the same length (21 bp), the highest binding affinity by MucR1 was observed for the one carrying motif_b_8 (AT% = 85%), followed by the other fragments carrying motif_b_5, motif_b_6, motif_b_7, motif_b_1(2), motif_b_3, or motif_b_4 (AT% = 54–77%; Supplementary Figure S5 and Supplementary Figure S6). Overall, MucR1 recruitment efficiency decreased with the increase of DNA GC content. These results provide strong evidence for the potential of this *Puxs1* probe to extensively interact with MucR1.

This information allowed us to perform further DNA-bridging assay (Figure 6B), in which biotin-labeled DNA probe is associated with the streptavidin magnetic beads and Cy5-labeled DNA probe can be bridged to bead-associated DNA by DNA-bridging proteins. The whole *Puxs1* fragment was roughly split in half: the 108-bp fragment I and 120-bp fragment II (Figure 6A and C). MucR1 can bridge the fragment I (or II) anchored on beads and the Cy5-labeled fragment I (or II) in the reaction buffer. MucR1 can also bridge the bead-anchored fragment II and the Cy5-labeled fragment I (Figure 6D). The Cy5-*Puxs1* probe not engaged in DNA-MucR1-DNA bridging was not all free as revealed in EMSA of supernatant samples (Figure 6E). There are two phased A-tracts (5'-AAAAAA-3' and 5'-ATTT-3') and four TpA steps between motif_a_3 and motif_b_5 (Figure 6A). A-tract is defined as DNA sequences with three or more consecutive adenines and/or thymines without the TpA step (82). It has been demonstrated that phased short A-tracts (with individual tracts <10 bp) induce a static intrinsic bending in the DNA double-helix (83,84). Moreover, the TpA step is the most flexible dinucleotide step contributing to DNA helix bending (85). Here we further tested to what extent the two phased A-tracts (5'-AAAAAA-3' and 5'-ATTT-3') may be involved in the observed DNA bridging mediated by MucR1 dimers or multimers. Two phased A-tracts were mutated from 5'-AAAAAA-3' and 5'-ATTT-3' to 5'-AACAAC-3' and 5'-ATCT-3', generating a mutated 228-bp *Puxs1* which was as efficient as the wild-type *Puxs1* in DNA-bridging assay using MucR1 (Supplementary Figure S8). Therefore, MucR1 does not rely on A-tracts to bridge DNA.

In contrast to MucR1, MucR1_{Y24G} exhibited significant defects in DNA bridging (Figure 6D), despite its ability of binding multiple sites of the Cy5-labeled *Puxs1* probe in the supernatant (Figure 6E, central panel). Since a proportion of the MucR1 pool was trapped in DNA-MucR1-DNA complex on beads while MucR1_{Y24G} was not (Figure 6D), there were more MucR1_{Y24G} than MucR1 available for EMSA of supernatant samples (Figure 6E). Therefore, the NTD-dependent self-association of MucR1 is essential for DNA-MucR1-DNA bridging complex formation (Figure 6F). As described above, the predicted MucR1 multimers have a quasi-circular structure with their NTDs associating inside and CTDs arranged along an outside ring (Figure 3 and Supplementary Figure S1), which seems to be different from those multimers of H-NS, Lsr2, MvaT and Rok with their CTDs arranged on two sides of the associating

NTD backbone (Supplementary Figure S1) (19). It is notable however that the low complex linker region between zinc-finger and N-terminal associating α helices may allow certain flexibility of MucR1 dimer and multimer during the interaction with DNA (Figure 6F).

Moreover, -10 element lies in the high-affinity region containing motif_b_8 and the region covering -35 element can also be effectively bound by MucR1 (Figure 6A, Supplementary Figures S5-S7), which together with downstream DNA-bridging events may prevent transcription initiation and/or elongation by RNA polymerase complex. This is supported by earlier evidence that the *uxs1* gene is significantly upregulated in the *mucR* mutants of both SF45436 and *Sinorhizobium meliloti* (28,46,86).

The essential role of MucR1 and/or its NTD in rhizobium-legume symbiosis can be replaced by non-homologous convergent silencers and/or their NTDs

The divergence of various rhizobial genera belonging to α -proteobacteria predates the emergence of legume and symbiotic nitrogen fixation (87–89). We have demonstrated that MucR1, conserved in α -proteobacteria, is essential for maintaining nitrogen fixation efficiency of rhizobia in legume nodules (20,46). Since the observed ever-increasing diversity of rhizobia (more than two hundred species) is largely attributable to the horizontal transfer of AT-rich symbiosis genes (90), we wondered if the convergently evolved xenogeneic silencing function of MucR (17,20) predisposed α -proteobacteria to successfully integrate horizontally acquired AT-rich symbiosis genes. To test this hypothesis, H-NS from *E. coli* (Gram-), Lsr2 from *M. tuberculosis* (Gram+), and various MucR1 derivatives with either NTD or CTD replaced by corresponding fragments from H-NS or Lsr2 were introduced into the chromosome of the Δ *mucR1&2* mutant of SF45436 as a single copy, which is under the control of the wild-type *PmucR1* promoter (Figure 7A). The Δ *mucR1&2* mutant carrying Lsr2 was not obtained due to the potentially lethal effect. Lsr2_(1–50) and Lsr2_(1–65) when fused with CTD of H-NS can complement phenotypes of the *hns* mutant of *E. coli* to a different extent (14), and therefore these two NTD fragments of Lsr2 were explored herein to generate the Δ *mucR1&2* mutant carrying Lsr2_{NTD}-MucR1_{CTD}.

Successful expression of H-NS and various chimeric MucR1 derivatives in the Δ *mucR1&2* mutant was verified by the *in vivo* cross-linking assay (Figure 7B), and self-association in the dimer form can be observed for H-NS, H-NS_(1–89)-MucR1_{CTD}, Lsr2_(1–65)-MucR1_{CTD}, MucR1_{NTD}-H-NS_(77–137), and MucR1_{NTD}-Lsr2_(74–112), but not for Lsr2_(1–50)-MucR1_{CTD}. It has been revealed that MucR1 is required for exopolysaccharide production and nitrogen fixation by directly modulating the transcription of exopolysaccharide biosynthesis genes and functional genes essential for maintaining nitrogen fixation process (32,38,46,91,92). The Δ *mucR1&2* mutant of SF45436 is characterized by forming non-mucoid colonies, and small nodules of low nitrogenase activity which led to a significant reduction in leaf chlorophyll content of soybean plants (38,46) (Figure 7C, D). H-NS, H-NS_(1–89)-MucR1_{CTD},

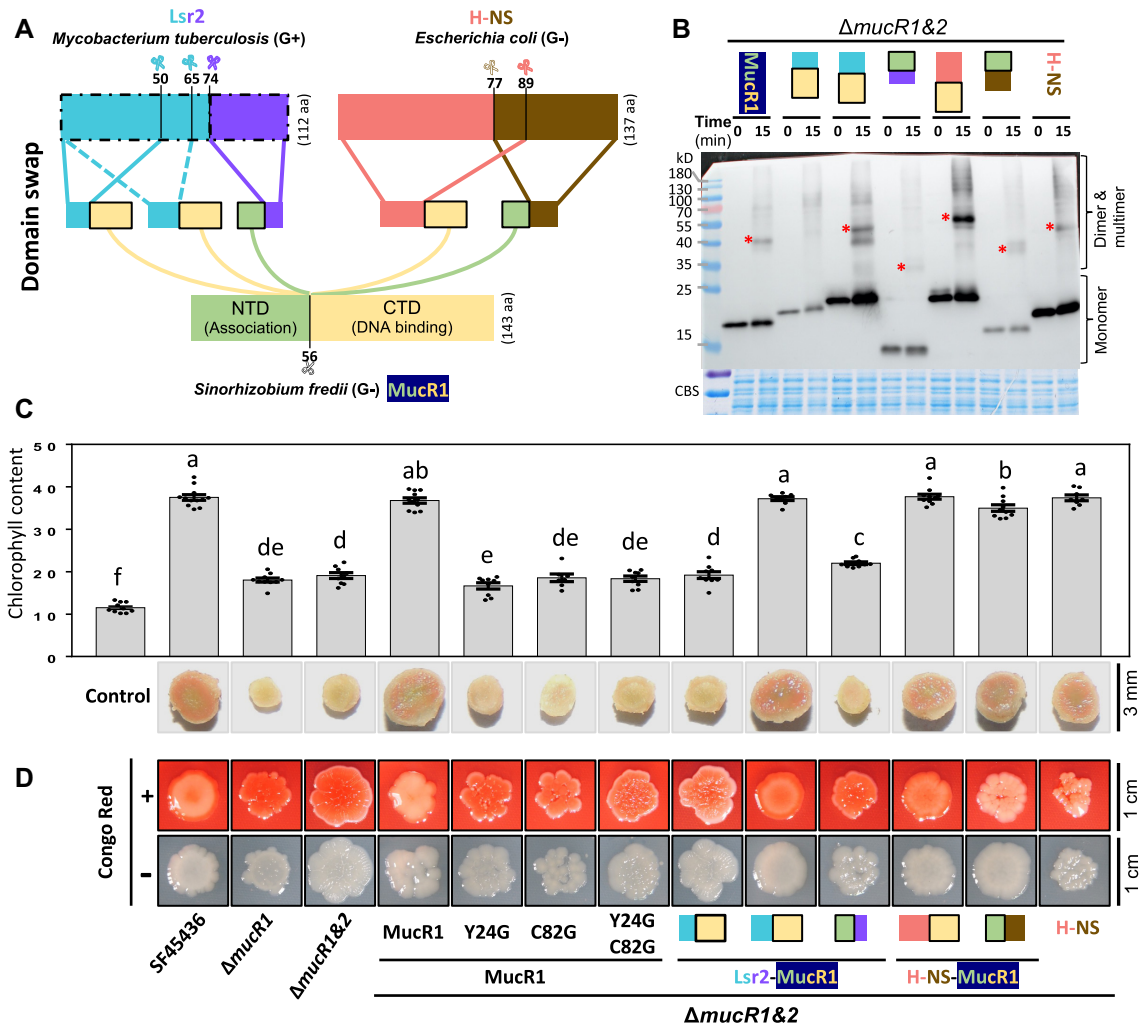


Figure 7. Convergent xenogeneic silencers can rescue symbiotic defects of the $\Delta mucR1\&2$ mutant. (A) Schematic diagram of domain swap among convergent xenogeneic silencers Lsr2, H-NS and MucR1. (B) *In vivo* cross-linking experiment of the $\Delta mucR1\&2$ mutant derivatives carrying MucR1-FLAG, Lsr2₍₁₋₅₀₎-MucR1_{CTD}-FLAG, Lsr2₍₁₋₆₅₎-MucR1_{CTD}-FLAG, MucR1_{NTD}-Lsr2₍₇₄₋₁₁₂₎-FLAG, H-NS₍₁₋₈₉₎-MucR1_{CTD}-FLAG, MucR1_{NTD}-H-NS₍₇₇₋₁₃₇₎-FLAG or H-NS-FLAG. (C) Symbiotic performance of the $\Delta mucR1\&2$ mutant derivatives on wild soybean plants. Leaf chlorophyll content and vertical section of nodules are displayed. Different letters indicate significant differences between means (mean \pm SEM; ANOVA followed by Duncan's test, $\alpha = 0.05$) of 7–12 plants. (D) Colony phenotypes of test strains on MOPS-buffered MM medium with or without Congo Red.

Lsr2₍₁₋₆₅₎-MucR1_{CTD}, MucR1_{NTD}-H-NS₍₇₇₋₁₃₇₎ rather than Lsr2₍₁₋₅₀₎-MucR1_{CTD} and MucR1_{NTD}-Lsr2₍₇₄₋₁₁₂₎ can effectively rescue the symbiotic performance of the $\Delta mucR1\&2$ mutant on soybean plants (Figure 7C). The red non-mucoid colony phenotype of the $\Delta mucR1\&2$ mutant on the minimum medium containing Congo Red can be largely rescued by H-NS₍₁₋₈₉₎-MucR1_{CTD} and Lsr2₍₁₋₆₅₎-MucR1_{CTD}, and to a less extent by MucR1_{NTD}-H-NS₍₇₇₋₁₃₇₎ and H-NS (Figure 7D). MucR1_{C82G} and MucR1_{Y24G} were not able to restore the symbiotic and colony phenotypes of the $\Delta mucR1\&2$ mutant (Figure 7C and D). These results demonstrated that NTD of MucR1 can be replaced by Lsr2₍₁₋₆₅₎ and H-NS₍₁₋₈₉₎ while H-NS₍₇₇₋₁₃₇₎ but not Lsr2₍₇₄₋₁₁₂₎ can functionally complement CTD of MucR1 *in vivo*. Therefore, convergently evolved xenogeneic silencers H-NS and Lsr2 can fully or partially complement the essential role of MucR1 in rhizobium-legume symbiosis.

MucR1, H-NS, and functional chimeric silencers share similar recruitment profiles in rhizobial genome

To further explore mechanisms underlying phenotype differences among these $\Delta mucR1\&2$ derivatives carrying foreign or chimeric silencers, ChIP-seq analyses were performed (Figure 8A). H-NS, H-NS₍₁₋₈₉₎-MucR1_{CTD}, Lsr2₍₁₋₆₅₎-MucR1_{CTD}, and MucR1_{NTD}-H-NS₍₇₇₋₁₃₇₎ had similar recruitment profiles across the multipartite genome of SF45436 while Lsr2₍₁₋₅₀₎-MucR1_{CTD}, MucR1_{NTD}-Lsr2₍₇₄₋₁₁₂₎, MucR1_{Y24G} and MucR1_{C82G} didn't show significant recruitment signals. These results were confirmed by ChIP-qPCR analyses of *Puxs1* and *PmucR1* (Supplementary Figure S9). Recruitment profiles were highly reproducible in three independent biological replicates (Supplementary Figure S10). Targets specific to individual wild-type or chimeric silencers had significantly less recruitment levels than those shared by multiple silencers (Figure 8B, C; Supplementary Figure S11). The

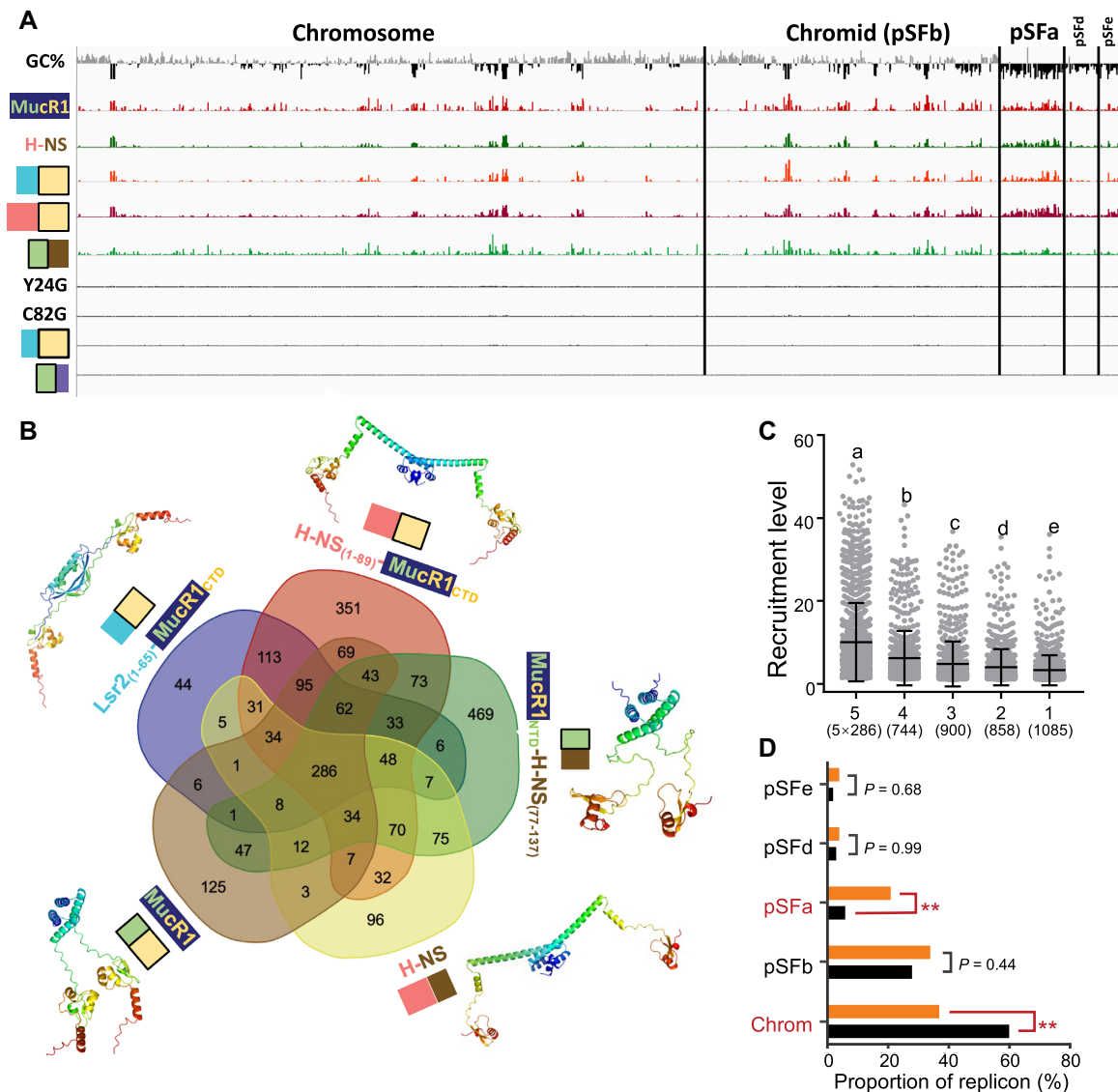


Figure 8. ChIP-seq of the $\Delta mucR1\&2$ mutant derivatives harboring convergent xenogeneic silencers. (A) ChIP-seq analysis showing recruitment levels of MucR1-FLAG, H-NS-FLAG, Lsr2₍₁₋₆₅₎-MucR1_{CTD}-FLAG, H-NS₍₁₋₈₉₎-MucR1_{CTD}-FLAG, MucR1_{NTD}-H-NS₍₇₇₋₁₃₇₎-FLAG, MucR1_{Y24G}-FLAG, MucR1_{C82G}-FLAG, Lsr2₍₁₋₅₀₎-MucR1_{CTD}-FLAG, or MucR1_{NTD}-Lsr2₍₇₄₋₁₁₂₎-FLAG in the $\Delta mucR1\&2$ mutant derivatives. The pooled ChIP-seq data from three independent biological replicates (Supplementary Figure S10) are shown. GC% below and above (black) and the genome average is indicated (window size 5000 bp). (B) Venn diagram showing the number of ChIP-seq peaks specific to each silencer or shared by different silencers. Predicted protein structures of homo-dimer by Alphafold2 are shown (the top 1 model based on local-distance difference test). (C) Silencer recruitment levels of ChIP-seq peaks specific to one strain (1) or shared by different strains (2–5). The number of peaks is shown in brackets. Different letters indicate significant differences between medians (Dunn's test, $\alpha = 0.05$). Error bars represent SD of mean. Results for individual strains are shown in Supplementary Figure S11. (D) Enrichment analysis of 286 common peak-associated genes regarding replicons. Orange and black bars represent proportions of common peak-associated genes and genome size, respectively. Significant enrichment/depletion is indicated (** P value < 0.01; chi-square test).

targets of high recruitment levels were generally located in AT-rich genomic regions (Figure 8A) and enriched in the symbiosis plasmid but depleted in the chromosome (Figure 8D). This is consistent with that DNA binding preferences of xenogeneic silencers Lsr2, H-NS, MvaT, Rok and MucR1 are positively correlated to the AT% of DNA sequences (17,38). Despite that NTDs from MucR1, H-NS and Lsr2 show no sequence homology (20), all of them can mediate self-association as demonstrated in cross-linking assay (Figure 7B) and structure prediction by Alphafold2 (Figure 8B). This allowed the DNA-binding domain either

from MucR1 or H-NS to effectively target similar AT-rich genomic regions of SF45436 (Figure 8A, C and D). Among the genes associated with 286 shared ChIP-seq peaks (Figure 8D), 144 genes have COG annotation (Supplementary Figure S12). This list includes MucR1 (chromosome), MucR2 (pSFa), and those involved in exopolysaccharide biosynthesis (*uxs1* and *exoY*; chromid), quorum sensing (TraI, TraR; pSymA), chemotaxis (VisN; chromosome), nodulation signal biosynthesis and regulation (NodU, NodO, NodE and NodD2; pSFa), type III secretion system (T3SS) components, effector and transcriptional

activator (RhcL, RhcT, RhcS, NolU, NopP and TtsI; pSFa), iron responsive regulator RirA, bacterioferritin and iron transporter (chromosome). In *S. fredii*, NodD2 is a negative regulator for the biosynthesis of nodulation signal lipochitooligosaccharide that induces nodulation process in host root (93); the effector protein NopP secreted by T3SS can modulate the host range (48,94); RirA is required for efficient nitrogen fixation in soybean nodules (91,95). The ability of MucR1, H-NS, H-NS₍₁₋₈₉₎-MucR1_{CTD}, Lsr2₍₁₋₆₅₎-MucR1_{CTD} and MucR1_{NTD}-H-NS₍₇₇₋₁₃₇₎ to target these genes and allow SF45436 to establish efficient symbiosis with soybean plants provides strong evidence for that the convergently evolved xenogeneic silencer predisposed α -proteobacteria to integrate horizontally transferable symbiosis genes.

It remains elusive why chimeric proteins with CTD from H-NS rather than that from Lsr2 work *in vivo* in the Δ *mucR1&2* mutant of SF45436. Indeed, we failed to obtain MucR1_{NTD}-Lsr2₍₅₁₋₁₁₂₎ and full-length Lsr2 complementary strains in the Δ *mucR1&2* mutant background. ChIP-seq data (Figure 8) indicated that MucR1_{NTD}-Lsr2₍₇₄₋₁₁₂₎ had no apparent binding peaks in the SF45436 genome. EMSA was further performed to test whether Lsr2, MucR1_{NTD}-Lsr2₍₅₁₋₁₁₂₎ and MucR1_{NTD}-Lsr2₍₇₄₋₁₁₂₎ could be recruited by *Puxs1* *in vitro* (Supplementary Figure S13). The data showed that Lsr2 and MucR1_{NTD}-Lsr2₍₅₁₋₁₁₂₎ had stronger DNA binding capacity compared to MucR1 throughout the test gradient of protein:DNA ratios (Supplementary Figure S13). In the treatment of Lsr2 and MucR1_{NTD}-Lsr2₍₅₁₋₁₁₂₎, the corresponding protein-DNA complexes were even stuck in the gel wells. It is likely that such strong protein-DNA interactions may lead to the lethal effect of MucR1_{NTD}-Lsr2₍₅₁₋₁₁₂₎ and Lsr2 in SF45436. By contrast, MucR1_{NTD}-Lsr2₍₇₄₋₁₁₂₎ exhibited a reduced bandshift than MucR1 at high protein:DNA ratios (Supplementary Figure S13), suggesting fewer proteins bound to the DNA probe. This is in line with its weak dimer signals *in vivo* (Figure 7B). Similarly, Lsr2₍₁₋₅₀₎-MucR1_{CTD} and MucR1_{Y24G} showing dimer-forming defects *in vivo* (Figure 7B) could not be effectively recruited to DNA in ChIP-seq (Figure 8). Therefore, MucR1 derivatives with defects in dimer assembly exhibited impaired DNA binding ability *in vitro* (Figure 4D, Supplementary Figure S3, and Supplementary Figure S13) and their interactions with DNA *in vivo* might be too fragile to be detected by the standard ChIP assay (Figure 8A and Supplementary Figure S9). Anyway, the *in vitro* evidence for CTD-DNA interactions (27,55) should be carefully addressed when their physiological relevance is discussed. By contrast, the stability and self-association of MucR1 can be ensured by its own NTD, Lsr2₍₁₋₆₅₎, or H-NS₍₁₋₈₉₎ (Figure 7B) and H-NS₍₁₋₈₉₎-MucR1_{CTD} and Lsr2₍₁₋₆₅₎-MucR1_{CTD} can largely restore symbiotic defects and colony phenotypes of the Δ *mucR1&2* mutant (Figure 7C and D).

MucR1 complements characteristic phenotypes of the Δ *hns* mutant of *E. coli*

To further test if MucR from α -proteobacteria can convergently function in γ -proteobacteria as Lsr2 from Gram+ *Mycobacterium*, *mucR1* from *S. fredii* was intro-

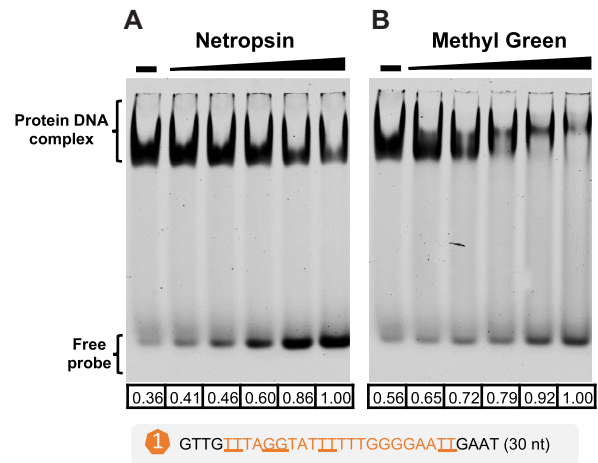


Figure 9. EMSA showing that MucR1 binds both minor and major grooves of DNA. Release of free probe from MucR1-DNA complex by minor-groove binding reagent netropsin (A) or major-groove binding reagent methyl green (B). Netropsin/methyl green concentration: 10, 20, 40, 80, 160 nM; ‘-’, 0 nM. MucR1 concentration: 10 μ M; DNA probe harboring motif α 1 of *Puxs1*: 10 nM. The numbers below each lane refer to quantified band intensity values of free probes that were calculated by Evolution-Capt Edge software.

duced into the Δ *hns* mutant of *E. coli* (66). The Δ *hns* mutant of *E. coli* has a characteristic mucoid colony phenotype and generates a clear zone around its colony on the blood agar plate due to hemolysis activity, which can be complemented by Lsr2 from Gram+ *Mycobacterium* (13). In this work, these characteristic phenotypes of the Δ *hns* mutant of *E. coli* can be fully complemented by H-NS, Lsr2 and MucR1, and partially by Lsr2₍₁₋₆₅₎-MucR1_{CTD}, MucR1_{NTD}-Lsr2₍₅₁₋₁₁₂₎ and MucR1_{NTD}-Lsr2₍₇₄₋₁₁₂₎ (Supplementary Figure S14). The protein expression was validated by Western blot using anti-FLAG antibody (Supplementary Figure S14). Therefore, MucR1 from α -proteobacteria and its various chimeric proteins with Lsr2 from Gram+ *Mycobacterium* can functionally replace H-NS in *E. coli*. These results strongly support that MucR1 is a convergently evolved xenogeneic silencer.

MucR1 contacts both minor and major grooves of target DNA

All known prokaryote xenogeneic silencers H-NS, Lsr2, MvaT and Rok bind the minor groove of DNA (17,18,20), while MucR1 and its close homolog Ros belong to the zinc-finger proteins which are well-known for their binding in the major groove in eukaryotes (54). The classic eukaryotic zinc-finger consists of a β -sheet and an α -helix ($\beta\beta\alpha$ fold) while the DNA binding domain of prokaryote Ros (Ros87) has a $\beta\beta\beta\alpha$ topology and two additional C-terminal basic regions (27). Similar to the classic zinc-finger, α 1 of Ros87 contacts the major groove of DNA (81), while notably the basic region in α 2 and two additional C-terminal basic regions make additional contacts with DNA and stabilize Ros87-DNA interaction (81). These three basic regions are essential for DNA binding ability of Ros87 *in vitro* (55). In this work (Figure 9), both minor-groove binding drug netropsin (Figure 9A) and major-groove binding drug

methyl green (Figure 9B) can impair the binding of MucR1 to a test fragment of *Puxs1*. Therefore, MucR1 has the ability to bind both major and minor grooves of DNA. Taken together, the following working model can be proposed: the first α -helix $\alpha 1$ in the zinc-finger structure of Ros/MucR is inserted into the major groove of DNA, and its C-terminal basic regions stabilize protein-DNA interaction by allowing Ros/MucR to bind DNA more extensively from the major groove to the minor groove of DNA.

CONCLUSION

This work reveals that the xenogeneic silencer MucR conserved in α -proteobacteria (20,38) is a novel DNA bridger with its NTD acting as a major modulator. The NTDs from more than 2000 MucR homologs have evolved conserved key residues and their spacer length to ensure self-association (Figure 1 and Figure 2). The NTD-dependent self-association can be enhanced by target DNA (*in vivo* and *in vitro*; Figure 3 and Figure 5), and is crucial for maintaining MucR stability (*in vivo*; Figure 4), transcriptional silencing (*in vivo*; Figure 4), and DNA–MucR–DNA bridging complex formation (*in vitro*; Figure 6). Like Lsr2 from *M. tuberculosis*, MucR can functionally complement H-NS in *E. coli* (Figure S14). On the other hand, NTDs from H-NS and Lsr2 can functionally replace the NTD of MucR regarding *in vivo* self-association (Figure 7) and symbiotic interaction of *S. fredii* with soybean plants (Figure 7). Moreover, the full-length H-NS can also rescue the symbiotic defect of the *mucR* mutant of *S. fredii* (Figure 7). H-NS and functional chimeric MucR derivatives have similar recruitment profiles across the multipartite genome of *S. fredii*, preferring AT-rich genomic islands and symbiosis plasmid, with key symbiosis genes as shared targets (Figure 8 and Supplementary Figure S12). Therefore, the convergently evolved xenogeneic silencer MucR conserved in α -proteobacteria is crucial for the successful integration of later acquired symbiosis genes, horizontal transfer of which is strongly selected in nature (96–98). Notably, functional MucR homologs can be found in symbiosis plasmids of diverse rhizobial species and bacterial phages (20,46), both of which can be horizontally transferred in microbiota (99,100). Since the AT-rich symbiosis genes in symbiosis plasmid are specifically transcribed during symbiotic interactions with legumes rather than under free-living conditions (101,102), it is intriguing to hypothesize that co-transfer of MucR with AT-rich sequences can be an adaptive mechanism by banking foreign genetic materials to fuel the process of exploring novel niches while maintaining regulatory integration. This may at least partially explain the successful spreading of symbiosis genes among hundreds of bacterial species in α -proteobacteria (90).

Since α -proteobacterium is enriched with both symbiotic and pathogenic bacteria associated with eukaryotes and had a putative ancestor for mitochondria (21), the working mechanisms of zinc-finger bearing DNA bridger MucR are of significant importance. The interaction between H-NS-like proteins and DNA can respond to various physico-chemical environmental signals, and diverse anti-silencing mechanisms have been reported (18,103–105). Among hundreds of direct targets of MucR in the mul-

tipartite genome of facultative microsymbiont *Sinorhizobium fredii* (38), many functional genes are involved in stress adaptation or symbiotic interactions (32,48,88,91,106), in which silencing and anti-silencing mechanisms remain unknown. Our current understanding of the biology of MucR in α -proteobacteria is just the tip of the iceberg.

DATA AVAILABILITY

Raw sequence data from ChIP-seq analyses can be accessed via NCBI Sequence Read Archive (PRJNA775862).

SUPPLEMENTARY DATA

Supplementary Data are available at NAR Online.

ACKNOWLEDGEMENTS

We thank Prof. Huiqiang Lou and Ertao Wang, and Dr Lili Li and Dapeng Wang for providing related strains and vectors used in yeast-two-hybrid assay. We thank Associate Prof. Dongchang Sun and Dr Mingyue Fei for providing related strains used in the *E. coli* phenotype assay.

Author contributions: C.-F.T. conceived the project. C.-F.T. and J.J. designed the research plan. W.-T.S. did all experiments with contribution from M.-L.L. W.-T.S., B.Z., J.J. and C.-F.T. analyzed data. W.-T.S. and C.-F.T. visualized data. C.-F.T., J.J. and W.-T.S. prepared the manuscript. C.-F.T. reviewed and edited the manuscript. All authors approved the final version.

FUNDING

National Key Research and Development Program of China [2019YFA09004700]; National Natural Science Foundation of China [32070078]; Innovative Project of State Key Laboratory of Agrobiotechnology [2020SKLAB1-5]; 2115 Talent Development Program of China Agricultural University. Funding for open access charge: National Natural Science Foundation of China.

Conflict of interest statement. None declared.

REFERENCES

- López-García, P. and Moreira, D. (2020) Cultured Asgard archaea shed light on eukaryogenesis. *Cell*, **181**, 232–235.
- Imachi, H., Nobu, M.K., Nakahara, N., Morono, Y., Ogawara, M., Takaki, Y., Takano, Y., Uematsu, K., Ikuta, T., Ito, M. *et al.* (2020) Isolation of an archaeon at the prokaryote–eukaryote interface. *Nature*, **577**, 519–525.
- Lane, N. (2020) How energy flow shapes cell evolution. *Curr. Biol.*, **30**, R471–R476.
- Ryan, D.G., Frezza, C. and Neill, L.A.J.O. (2021) TCA cycle signalling and the evolution of eukaryotes. *Curr. Opin. Biotechnol.*, **68**, 72–88.
- Brunk, C.F. and Martin, W.F. (2019) Archaeal histone contributions to the origin of eukaryotes. *Trends Microbiol.*, **27**, 703–714.
- McInerney, J.O., McNally, A. and O’Connell, M.J. (2017) Why prokaryotes have pangenomes. *Nat. Microbiol.*, **2**, 17040.
- Dame, R.T., Rashid, F.Z.M. and Grainger, D.C. (2020) Chromosome organization in bacteria: mechanistic insights into genome structure and function. *Nat. Rev. Genet.*, **21**, 227–242.
- Badrinarayanan, A., Le, T.B.K. and Laub, M.T. (2015) Bacterial chromosome organization and segregation. *Annu. Rev. Cell Dev. Biol.*, **31**, 171–199.

9. Nolivos,S. and Sherratt,D. (2014) The bacterial chromosome: architecture and action of bacterial SMC and SMC-like complexes. *FEMS Microbiol. Rev.*, **38**, 380–392.
10. Navarre,W.W., Porwollik,S., Wang,Y., McClelland,M., Rosen,H., Libby,S.J. and Fang,F.C. (2006) Selective silencing of foreign DNA with low GC content by the H-NS protein in *Salmonella*. *Science*, **313**, 236–238.
11. Tendeng,C., Soutourina,O.A., Danchin,A. and Bertin,P.N. (2003) MvaT proteins in *Pseudomonas* spp.: a novel class of H-NS-like proteins. *Microbiology*, **149**, 3047–3050.
12. Ding,P., McFarland,K.A., Jin,S., Tong,G., Duan,B., Yang,A., Hughes,T.R., Liu,J., Dove,S.L., Navarre,W.W. et al. (2015) A novel AT-rich DNA recognition mechanism for bacterial xenogeneic silencer MvaT. *PLoS Pathog.*, **11**, e1004967.
13. Gordon,B.R.G., Imperial,R., Wang,L., Navarre,W.W. and Liu,J. (2008) Lsr2 of *Mycobacterium* represents a novel class of H-NS-like proteins. *J. Bacteriol.*, **190**, 7052–7059.
14. Gordon,B.R.G., Li,Y., Wang,L., Sintsova,A., van Bakel,H., Tian,S., Navarre,W.W., Xia,B. and Liu,J. (2010) Lsr2 is a nucleoid-associated protein that targets AT-rich sequences and virulence genes in *Mycobacterium tuberculosis*. *Proc. Natl. Acad. Sci. U.S.A.*, **107**, 5154–5159.
15. Smits,W.K. and Grossman,A.D. (2010) The transcriptional regulator Rok binds A+T-rich DNA and is involved in repression of a mobile genetic element in *Bacillus subtilis*. *PLoS Genet.*, **6**, e1001207.
16. Marbouty,M., Le Gall,A., Cattoni,D.I., Cournac,A., Koh,A., Fiche,J.B., Mozziconacci,J., Murray,H., Koszul,R. and Nollmann,M. (2015) Condensin- and replication-mediated bacterial chromosome folding and origin condensation revealed by Hi-C and super-resolution imaging. *Mol. Cell*, **59**, 588–602.
17. Duan,B., Ding,P., Navarre,W.W., Liu,J. and Xia,B. (2021) Xenogeneic silencing and bacterial genome evolution: mechanisms for DNA recognition imply multifaceted roles of xenogeneic silencers. *Mol. Biol. Evol.*, **38**, 4135–4148.
18. Singh,K., Milstein,J.N. and Navarre,W.W. (2016) Xenogeneic silencing and its impact on bacterial genomes. *Annu. Rev. Microbiol.*, **70**, 199–213.
19. Qin,L., Erkelens,A.M., Ben Bdira,F. and Dame,R.T. (2019) The architects of bacterial DNA bridges: a structurally and functionally conserved family of proteins. *Open Biol.*, **9**, 190223.
20. Jiao,J. and Tian,C.-F. (2020) Ancestral zinc-finger bearing protein MucR in alpha-proteobacteria: a novel xenogeneic silencer? *Comput. Struct. Biotechnol. J.*, **18**, 3623–3631.
21. Batut,J., Andersson,S.G. and O’Callaghan,D. (2004) The evolution of chronic infection strategies in the alpha-proteobacteria. *Nat. Rev. Microbiol.*, **2**, 933–945.
22. Close,T.J., Tait,R.C. and Kado,C.I. (1985) Regulation of Ti plasmid virulence genes by a chromosomal locus of *Agrobacterium tumefaciens*. *J. Bacteriol.*, **164**, 774–781.
23. Zhan,H.J., Levery,S.B., Lee,C.C. and Leigh,J.A. (1989) A second exopolysaccharide of *Rhizobium meliloti* strain SU47 that can function in root nodule invasion. *Proc. Natl. Acad. Sci. U.S.A.*, **86**, 3055–3059.
24. Keller,M., Roxlau,A., Weng,W.M., Schmidt,M., Quandt,J., Niehaus,K., Jording,D., Arnold,W. and Puhler,A. (1995) Molecular analysis of the *Rhizobium meliloti mucR* gene regulating the biosynthesis of the exopolysaccharides succinoglycan and galactoglucan. *Mol. Plant-Microbe Interact.*, **8**, 267–277.
25. Bittinger,M.A., Milner,J.L., Saville,B.J. and Handelsman,J. (1997) *rosR*, a determinant of nodulation competitiveness in *Rhizobium etli*. *Mol. Plant-Microbe Interact.*, **10**, 180–186.
26. Janczarek,M. and Skorupska,A. (2007) The *Rhizobium leguminosarum* bv. *trifolii* RosR: transcriptional regulator involved in exopolysaccharide production. *Mol. Plant-Microbe Interact.*, **20**, 867–881.
27. Malgieri,G., Russo,L., Esposito,S., Baglivo,I., Zaccaro,L., Pedone,E.M., Di Blasio,B., Isernia,C., Pedone,P.V. and Fattorusso,R. (2007) The prokaryotic Cys₂His₂ zinc-finger adopts a novel fold as revealed by the NMR structure of *Agrobacterium tumefaciens* Ros DNA-binding domain. *Proc. Natl. Acad. Sci. U.S.A.*, **104**, 17341–17346.
28. Schäper,S., Wendt,H., Bamberger,J., Sieber,V., Schmid,J. and Becker,A. (2019) A bifunctional UDP-Sugar 4-epimerase supports biosynthesis of multiple cell surface polysaccharides in *Sinorhizobium meliloti*. *J. Bacteriol.*, **201**, e00801-18.
29. Bertram-Drogatz,P.A., Quester,I., Becker,A. and Puhler,A. (1998) The *Sinorhizobium meliloti* MucR protein, which is essential for the production of high-molecular-weight succinoglycan exopolysaccharide, binds to short DNA regions upstream of *exoH* and *exoY*. *Mol. Gen. Genet.*, **257**, 433–441.
30. Janczarek,M. and Skorupska,A. (2011) Modulation of *rosR* expression and exopolysaccharide production in *Rhizobium leguminosarum* bv. *trifolii* by phosphate and clover root exudates. *Int. J. Mol. Sci.*, **12**, 4132–4155.
31. Fumeaux,C., Radhakrishnan,S.K., Ardisson,S., Théraulaz,L., Frandi,A., Martins,D., Nesper,J., Abel,S., Jenal,U. and Viollier,P.H. (2014) Cell cycle transition from S-phase to G1 in *Caulobacter* is mediated by ancestral virulence regulators. *Nat. Commun.*, **5**, 4081.
32. Li,M.-L., Jiao,J., Zhang,B., Shi,W.-T., Yu,W.-H. and Tian,C.-F. (2021) Global transcriptional repression of diguanylate cyclases by MucR1 is essential for *Sinorhizobium*-soybean symbiosis. *mBio*, **12**, e01192-21.
33. Bahlawane,C., McIntosh,M., Krol,E. and Becker,A. (2008) *Sinorhizobium meliloti* regulator MucR couples exopolysaccharide synthesis and motility. *Mol. Plant-Microbe Interact.*, **21**, 1498–1509.
34. Rachwał,K., Matczyńska,E. and Janczarek,M. (2015) Transcriptome profiling of a *Rhizobium leguminosarum* bv. *trifolii* *rosR* mutant reveals the role of the transcriptional regulator RosR in motility, synthesis of cell-surface components, and other cellular processes. *BMC Genomics*, **16**, 1111.
35. Janczarek,M., Kutkowska,J., Piersiak,T. and Skorupska,A. (2010) *Rhizobium leguminosarum* bv. *trifolii* *rosR* is required for interaction with clover, biofilm formation and adaptation to the environment. *BMC Microbiol.*, **10**, 284.
36. Mueller,K. and Gonzalez,J.E. (2011) Complex regulation of symbiotic functions is coordinated by MucR and quorum sensing in *Sinorhizobium meliloti*. *J. Bacteriol.*, **193**, 485–496.
37. Mirabella,A., Terwagne,M., Zygmunt,M.S., Cloeckeaert,A., De Bolle,X. and Letesson,J.J. (2013) *Brucella melitensis* MucR, an orthologue of *Sinorhizobium meliloti* MucR, is involved in resistance to oxidative, detergent, and saline stresses and cell envelope modifications. *J. Bacteriol.*, **195**, 453–465.
38. Jiao,J., Zhang,B., Li,M.-L., Zhang,Z. and Tian,C.-F. (2022) The zinc-finger bearing xenogeneic silencer MucR in α -proteobacteria balances adaptation and regulatory integrity. *ISME J.*, **16**, 738–749.
39. Jaboulay,C., Godeux,A.S., Doublet,P. and Vianney,A. (2021) Regulatory networks of the T4SS control: from host cell sensing to the biogenesis and the activity during the infection. *J. Mol. Biol.*, **433**, 166892.
40. Sun,J., Dong,H., Peng,X., Liu,Y., Jiang,H., Feng,Y., Li,Q., Zhu,L., Qin,Y. and Ding,J. (2021) Deletion of the transcriptional regulator MucR in *Brucellacanis* affects stress responses and bacterial virulence. *Front. Vet. Sci.*, **8**, 650942.
41. Borriello,G., Russo,V., Paradiso,R., Riccardi,M.G., Criscuolo,D., Verde,G., Marasco,R., Pedone,P.V., Galiero,G. and Baglivo,I. (2020) Different impacts of MucR binding to the *babR* and *virB* promoters on gene expression in *Brucella abortus* 2308. *Biomolecules*, **10**, 788.
42. Caswell,C.C., Elhassanny,A.E.M., Planchin,E.E., Roux,C.M., Weeks-Gorospe,J.N., Ficht,T.A., Dunman,P.M. and Martin Roop,R. (2013) Diverse genetic regulon of the virulence-associated transcriptional regulator MucR in *Brucella abortus* 2308. *Infect. Immun.*, **81**, 1040–1051.
43. Dong,H., Liu,W., Peng,X., Jing,Z. and Wu,Q. (2013) The effects of MucR on expression of type IV secretion system, quorum sensing system and stress responses in *Brucella melitensis*. *Vet. Microbiol.*, **166**, 535–542.
44. Cooley,M.B., D’Souza,M.R. and Kado,C.I. (1991) The *virC* and *virD* operons of the *Agrobacterium* Ti plasmid are regulated by the *ros* chromosomal gene: analysis of the cloned *ros* gene. *J. Bacteriol.*, **173**, 2608–2616.
45. Chou,A.Y., Archdeacon,J. and Kado,C.I. (1998) *Agrobacterium* transcriptional regulator Ros is a prokaryotic zinc finger protein that regulates the plant oncogene *ipt*. *Proc. Natl. Acad. Sci. U.S.A.*, **95**, 5293–5298.
46. Jiao,J., Wu,L.J., Zhang,B., Hu,Y., Li,Y., Zhang,X.X., Guo,H.J., Liu,L.X., Chen,W.X., Zhang,Z. et al. (2016) MucR is required for transcriptional activation of conserved ion transporters to support

- nitrogen fixation of *Sinorhizobium fredii* in soybean nodules. *Mol. Plant-Microbe Interact.*, **29**, 352–361.
47. Acosta-Jurado, S., Alias-Villegas, C., Navarro-Gomez, P., Zehner, S., Del Socorro Murdoch, P., Rodríguez-Carvajal, M.A., Soto, M.J., Ollero, F.J., Ruiz-Sainz, J.E., Göttfert, M. *et al.* (2016) The *Sinorhizobium fredii* HH103 MucR1 global regulator is connected with the *nod* regulon and is required for efficient symbiosis with *Lotus burttii* and *Glycine max* cv. Williams. *Mol. Plant-Microbe Interact.*, **29**, 700–712.
 48. Zhao, R., Liu, L.X., Zhang, Y.Z., Jiao, J., Cui, W.J., Zhang, B., Wang, X.L., Li, M.L., Chen, Y., Xiong, Z.Q. *et al.* (2018) Adaptive evolution of rhizobial symbiotic compatibility mediated by co-evolved insertion sequences. *ISME J*, **12**, 101–111.
 49. Yousof, M., Iuliani, I., Veetil, R.T., Seshasayee, A.S.N., Sclavi, B. and Cosentino Lagomarsino, M. (2020) Early fate of exogenous promoters in *E. coli*. *Nucleic Acids Res.*, **48**, 2348–2356.
 50. Lamberte, L.E., Baniulyte, G., Singh, S.S., Stringer, A.M., Bonocora, R.P., Stracy, M., Kapanidis, A.N., Wade, J.T. and Grainger, D.C. (2017) Horizontally acquired AT-rich genes in *Escherichia coli* cause toxicity by sequestering RNA polymerase. *Nat. Microbiol.*, **2**, 16249.
 51. Netti, F., Malgieri, G., Esposito, S., Palmieri, M., Baglivo, I., Isernia, C., Omichinski, J.G., Pedone, P.V., Lartillot, N. and Fattorusso, R. (2013) An experimentally tested scenario for the structural evolution of eukaryotic Cys₂His₂ zinc fingers from eubacterial Ros homologs. *Mol. Biol. Evol.*, **30**, 1504–1513.
 52. Baglivo, I., Russo, L., Esposito, S., Malgieri, G., Renda, M., Salluzzo, A., Di Blasio, B., Isernia, C., Fattorusso, R. and Pedone, P.V. (2009) The structural role of the zinc ion can be dispensable in prokaryotic zinc-finger domains. *Proc. Natl. Acad. Sci. U.S.A.*, **106**, 6933–6938.
 53. Sivo, V., D'Abrosca, G., Baglivo, I., Iacovino, R., Pedone, P.V., Fattorusso, R., Russo, L., Malgieri, G. and Isernia, C. (2019) Ni(II), Hg(II), and Pb(II) coordination in the prokaryotic zinc-finger Ros87. *Inorg. Chem.*, **58**, 1067–1080.
 54. Malgieri, G., Palmieri, M., Russo, L., Fattorusso, R., Pedone, P.V. and Isernia, C. (2015) The prokaryotic zinc-finger: structure, function and comparison with the eukaryotic counterpart. *FEBS J.*, **282**, 4480–4496.
 55. Esposito, S., Baglivo, I., Malgieri, G., Russo, L., Zaccaro, L., D'Andrea, L.D., Mammucari, M., Di Blasio, B., Isernia, C., Fattorusso, R. *et al.* (2006) A novel type of zinc finger DNA binding domain in the *Agrobacterium tumefaciens* transcriptional regulator Ros. *Biochemistry*, **45**, 10394–10405.
 56. Dathan, N., Zaccaro, L., Esposito, S., Isernia, C., Omichinski, J.G., Riccio, A., Pedone, C., Di Blasio, B., Fattorusso, R. and Pedone, P.V. (2002) The *Arabidopsis* SUPERMAN protein is able to specifically bind DNA through its single Cys₂-His₂ zinc finger motif. *Nucleic Acids Res.*, **30**, 4945–4951.
 57. Pedone, P.V., Ghirlando, R., Clore, G.M., Gronenborns, A.M., Felsenfeld, G. and Omichinski, J.G. (1996) The single Cys₂-His₂ zinc finger domain of the GAGA protein flanked by basic residues is sufficient for high-affinity specific DNA binding. *Proc. Natl. Acad. Sci. U.S.A.*, **93**, 2822–2826.
 58. Rodríguez, J., Learte-Aymami, S., Mosquera, J., Celaya, G., Rodríguez-Larrea, D., Vázquez, M.E. and Mascareñas, J.L. (2018) DNA-binding miniproteins based on zinc fingers. Assessment of the interaction using nanopores. *Chem. Sci.*, **9**, 4118–4123.
 59. Pirone, L., Pitzer, J.E., D'Abrosca, G., Fattorusso, R., Malgieri, G., Pedone, E.M., Pedone, P.V., Roop, R.M. and Baglivo, I. (2018) Identifying the region responsible for *Brucella abortus* MucR higher-order oligomer formation and examining its role in gene regulation. *Sci. Rep.*, **8**, 17238.
 60. Baglivo, I., Pirone, L., Pedone, E.M., Pitzer, J.E., Muscariello, L., Marino, M.M., Malgieri, G., Freschi, A., Chambéry, A., Roop, R.M. *et al.* (2017) Ml proteins from *Mesorhizobium loti* and MucR from *Brucella abortus*: an AT-rich core DNA-target site and oligomerization ability. *Sci. Rep.*, **7**, 15805.
 61. D'Abrosca, G., Paladino, A., Baglivo, I., Russo, L., Sassano, M., Grazioso, R., Iacovino, R., Pirone, L., Pedone, E.M., Pedone, P.V. *et al.* (2020) Structural insight of the full-length Ros protein: a prototype of the prokaryotic zinc-finger family. *Sci. Rep.*, **10**, 9283.
 62. Liu, L.X., Li, Q.Q., Zhang, Y.Z., Hu, Y., Jiao, J., Guo, H.J., Zhang, X.X., Zhang, B., Chen, W.X. and Tian, C.F. (2017) The nitrate-reduction gene cluster components exert lineage-dependent contributions to optimization of *Sinorhizobium* symbiosis with soybeans. *Environ. Microbiol.*, **19**, 4926–4938.
 63. Li, Y.Z., Wang, D., Feng, X.Y., Jiao, J., Chen, W.X. and Tian, C.F. (2016) Genetic analysis reveals the essential role of nitrogen phosphotransferase system components in *Sinorhizobium fredii* CCBAU 45436 symbioses with soybean and pigeonpea plants. *Appl. Environ. Microbiol.*, **82**, 1305–1315.
 64. Krol, E., Skotnicka, D., Kaever, V., Hilker, R. and Becker, A. (2016) Cyclic di-GMP regulates multiple cellular functions in the symbiotic alphaproteobacterium *Sinorhizobium meliloti*. *J. Bacteriol.*, **198**, 521–535.
 65. Quandt, J. and Hynes, M.F. (1993) Versatile suicide vectors which allow direct selection for gene replacement in Gram-negative bacteria. *Gene*, **127**, 15–21.
 66. Sun, D., Mao, X., Fei, M., Chen, Z., Zhu, T. and Qiu, J. (2020) Histone-like nucleoid-structuring protein (H-NS) paralogue StpA activates the type I-E CRISPR-Cas system against natural transformation in *Escherichia coli*. *Appl. Environ. Microbiol.*, **86**, e00731-20.
 67. Mirdita, M., Schütze, K., Moriawaki, Y., Heo, L., Ovchinnikov, S. and Steinegger, M. (2022). ColabFold: making protein folding accessible to all. *Nat Methods*, **19**, 679–682.
 68. Jumper, J., Evans, R., Pritzel, A., Green, T., Figurnov, M., Ronneberger, O., Tunyasuvunakool, K., Bates, R., Židek, A., Potapenko, A. *et al.* (2021) Highly accurate protein structure prediction with AlphaFold. *Nature*, **596**, 583–589.
 69. Kim, S.K. and Nordén, B. (1993) Methyl green. A DNA major-groove binding drug. *FEBS Lett.*, **315**, 61–64.
 70. Taberner, L., Verdaguer, N., Coll, M., Fita, I., van der Marel, G.A., van Boom, J.H., Rich, A. and Aymami, J. (1993) Molecular structure of the A-tract DNA dodecamer d(CGCAAATTTGCG) complexed with the minor groove binding drug netropsin. *Biochemistry*, **32**, 8403–8410.
 71. van der Valk, R.A., Vreede, J., Qin, L., Moolenaar, G.F., Hofmann, A., Goosen, N. and Dame, R.T. (2017) Mechanism of environmentally driven conformational changes that modulate H-NS DNA-bridging activity. *Elife*, **6**, e27369.
 72. Shindo, H., Iwaki, T., Ieda, R., Kurumuzaka, H., Ueguchi, C., Mizuno, T., Marikawa, S., Nakamura, H. and Kuboniwa, H. (1995) Solution structure of the DNA binding domain of a nucleoid-associated protein, H-NS, from *Escherichia coli*. *FEBS Lett.*, **360**, 125–131.
 73. Bloch, V., Yang, Y., Margeat, E., Chavanieu, A., Augé, M.T., Robert, B., Arold, S., Rimsky, S. and Kochoyan, M. (2003) The H-NS dimerization domain defines a new fold contributing to DNA recognition. *Nat. Struct. Biol.*, **10**, 212–218.
 74. Summers, E.L., Meindl, K., Usón, I., Mitra, A.K., Radjainia, M., Colangeli, R., Alland, D. and Arcus, V.L. (2012) The structure of the oligomerization domain of Lsr2 from *Mycobacterium tuberculosis* reveals a mechanism for chromosome organization and protection. *PLoS One*, **7**, e38542.
 75. Boyken, S.E., Benhaim, M.A., Busch, F., Jia, M., Bick, M.J., Choi, H., Klima, J.C., Chen, Z., Walkey, C., Mileant, A. *et al.* (2019) De novo design of tunable, pH-driven conformational changes. *Science*, **364**, 658–664.
 76. Rhys, G.G., Dawson, W.M., Beesley, J.L., Martin, F.J.O., Brady, R.L., Thomson, A.R. and Woolfson, D.N. (2021) How coiled-coil assemblies accommodate multiple aromatic residues. *Biomacromolecules*, **22**, 2010–2019.
 77. Chen, J.M., Ren, H., Shaw, J.E., Wang, Y.J., Li, M., Leung, A.S., Tran, V., Berbenetz, N.M., Kocincová, D., Yip, C.M. *et al.* (2008) Lsr2 of *Mycobacterium tuberculosis* is a DNA-bridging protein. *Nucleic Acids Res.*, **36**, 2123–2135.
 78. Dame, R.T., Luijsterburg, M.S., Krin, E., Bertin, P.N., Wagner, R. and Wuite, G.J.L. (2005) DNA bridging: a property shared among H-NS-like proteins. *J. Bacteriol.*, **187**, 1845–1848.
 79. Qin, L., Erkelens, A.M., Markus, D. and Dame, R.T. (2019) The *B. subtilis* Rok protein compacts and organizes DNA by bridging. *bioRxiv* doi: <https://doi.org/10.1101/769117>, 14 September 2019, preprint: not peer reviewed.
 80. Larsabal, E. and Danchin, A. (2005) Genomes are covered with ubiquitous 11 bp periodic patterns, the 'class A flexible patterns'. *BMC Bioinformatics*, **6**, 206.

81. Russo, L., Palmieri, M., Caso, J.V., Abrosca, G.D., Diana, D., Maligneri, G., Baglivo, I., Isernia, C., Pedone, P.V. and Fattorusso, R. (2015) Towards understanding the molecular recognition process in prokaryotic zinc-finger domain. *Eur. J. Med. Chem.*, **91**, 100–108.
82. Marin-Gonzalez, A., Vilhena, J.G., Perez, R. and Moreno-Herrero, F. (2021) A molecular view of DNA flexibility. *Q. Rev. Biophys.*, **54**, e8.
83. Marin-Gonzalez, A., Pastrana, C.L., Bocanegra, R., Martín-González, A., Vilhena, J.G., Pérez, R., Ibarra, B., Aicart-Ramos, C. and Moreno-Herrero, F. (2020) Understanding the paradoxical mechanical response of in-phase A-tracts at different force regimes. *Nucleic Acids Res.*, **48**, 5024–5036.
84. Koo, H.S., Wu, H.M. and Crothers, D.M. (1986) DNA bending at adenine · thymine tracts. *Nature*, **320**, 501–506.
85. Yodh, J.G., Ha, T., Ngo, T.T.M., Zhang, Q., Zhou, R., Yodh, J.G. and Ha, T. (2015) Asymmetric unwrapping of nucleosomes under tension directed by DNA local flexibility. *Cell*, **160**, 1135–1144.
86. Schäper, S., Steinchen, W., Krol, E., Altegoer, F., Skotnicka, D., Sogaard-Andersen, L., Bange, G. and Becker, A. (2017) AraC-like transcriptional activator CuxR binds c-di-GMP by a PilZ-like mechanism to regulate extracellular polysaccharide production. *Proc. Natl. Acad. Sci. U.S.A.*, **114**, e4822–e4831.
87. Turner, S.G. and Young, J.P.W. (2000) The glutamine synthetases of rhizobia: phylogenetics and evolutionary implications. *Mol. Biol. Evol.*, **17**, 309–319.
88. Cui, W., Zhang, B., Zhao, R., Liu, L., Jiao, J., Zhang, Z. and Tian, C.-F. (2021) Lineage-specific rewiring of core pathways predating innovation of legume nodules shapes symbiotic efficiency. *mSystems*, **6**, e01299-20.
89. Griesmann, M., Chang, Y., Liu, X., Song, Y., Haberger, G., Crook, M.B., Billault-Penneteau, B., Lauresergues, D., Keller, J., Imanishi, L. et al. (2018) Phylogenomics reveals multiple losses of nitrogen-fixing root nodule symbiosis. *Science*, **361**, eaat1743.
90. de Lajudie, P.M., Andrews, M., Ardley, J., Eardly, B., Jumas-bilak, E., Kuzmanović, N., Lassalle, F., Lindström, K., Mhamdi, R., Martínez-Romero, E. et al. (2019) Minimal standards for the description of new genera and species of rhizobia and agrobacteria. *Int. J. Syst. Evol. Microbiol.*, **69**, 1852–1863.
91. Liu, K.-H., Zhang, B., Yang, B.-S., Shi, W.-T., Li, Y.-F., Wang, Y., Zhang, P., Jiao, J. and Tian, C.-F. (2022) Rhizobiales-specific RirA represses a naturally ‘synthetic’ foreign siderophore gene cluster to maintain *Sinorhizobium*-legume mutualism. *mBio*, **13**, e02900-21.
92. Hu, Y., Jiao, J., Liu, L.X., Sun, Y.W., Chen, W., Sui, X., Chen, W. and Tian, C.F. (2018) Evidence for phosphate starvation of rhizobia without terminal differentiation in legume nodules. *Mol. Plant-Microbe Interact.*, **31**, 1060–1068.
93. Fellay, R., Hanin, M., Montorzi, G., Frey, J., Freiberg, C., Golinowski, W., Staehelin, C., Broughton, W.J. and Jabbouri, S. (1998) *nodD2* of *Rhizobium* sp. NGR234 is involved in the repression of the *nodABC* operon. *Mol. Microbiol.*, **27**, 1039–1050.
94. Rehman, H.M., Cheung, W.-L., Wong, K.-S., Xie, M., Luk, C.-Y., Wong, F.-L., Li, M.-W., Tsai, S.-N., To, W.-T., Chan, L.-Y. et al. (2019) High-throughput mass spectrometric analysis of the whole proteome and secretome from *Sinorhizobium fredii* strains CCBAU25509 and CCBAU45436. *Front. Microbiol.*, **10**, 2569.
95. Crespo-Rivas, J.C., Navarro-Gómez, P., Alias-Villegas, C., Shi, J., Zhen, T., Niu, Y., Cuéllar, V., Moreno, J., Cubo, T., Vinardell, J.M. et al. (2019) *Sinorhizobium fredii* HH103 RirA is required for oxidative stress resistance and efficient symbiosis with soybean. *Int. J. Mol. Sci.*, **20**, 787.
96. Ling, J., Wang, H., Wu, P., Li, T., Tang, Y., Naseer, N., Zheng, H., Masson-boivin, C., Zhong, Z. and Zhu, J. (2016) Plant nodulation inducers enhance horizontal gene transfer of *Azorhizobium caulinodans* symbiosis island. *Proc. Natl. Acad. Sci. U.S.A.*, **113**, 13875–13880.
97. Sullivan, J.T., Patrick, H.N., Lowther, W.L., Scott, D.B. and Ronson, C.W. (1995) Nodulating strains of *Rhizobium loti* arise through chromosomal symbiotic gene transfer in the environment. *Proc. Natl. Acad. Sci. U.S.A.*, **92**, 8985–8989.
98. Remigi, P., Zhu, J., Young, J.P.W. and Masson-Boivin, C. (2016) Symbiosis within symbiosis: evolving nitrogen-fixing legume symbionts. *Trends Microbiol.*, **24**, 63–75.
99. Nogales, J., Blanca-ordóñez, H., Olivares, J., Sanjuán, J. and Pérez-Mendoza, D. (2013) Conjugal transfer of the *Sinorhizobium meliloti* 1021 symbiotic plasmid is governed through the concerted action of one- and two-component signal transduction regulators. *Environ. Microbiol.*, **15**, 811–821.
100. Pérez-Mendoza, D., Sepúlveda, E., Pando, V., Muñoz, S., Nogales, J., Olivares, J., Soto, M.J., Herrera-Cervera, J.A., Romero, D., Brom, S. et al. (2005) Identification of the *retA* gene, which is required for repression of conjugative transfer of rhizobial symbiotic megaplasmids. *J. Bacteriol.*, **187**, 7341–7350.
101. Jiao, J., Ni, M., Zhang, B., Zhang, Z., Young, J.P.W., Chan, T.-F., Chen, W.X., Lam, H.-M. and Tian, C.F. (2018) Coordinated regulation of core and accessory genes in the multipartite genome of *Sinorhizobium fredii*. *PLoS Genet.*, **14**, e1007428.
102. Poole, P., Ramachandran, V. and Terpolilli, J. (2018) Rhizobia: from saprophytes to endosymbionts. *Nat. Rev. Microbiol.*, **16**, 291–303.
103. Choi, J. and Groisman, E.A. (2020) *Salmonella* expresses foreign genes during infection by degrading their silencer. *Proc. Natl. Acad. Sci. U.S.A.*, **117**, 8074–8082.
104. Wade, J.T. and Grainger, D.C. (2018) Waking the neighbours: disruption of H-NS repression by overlapping transcription. *Mol. Microbiol.*, **108**, 221–225.
105. Stoebel, D.M., Free, A. and Dorman, C.J. (2008) Anti-silencing: overcoming H-NS-mediated repression of transcription in Gram-negative enteric bacteria. *Microbiology*, **154**, 2533–2545.
106. Feng, X.-Y., Tian, Y., Cui, W.-J., Li, Y.-Z., Wang, D., Liu, Y., Jiao, J., Chen, W.-X. and Tian, C.-F. (2022) The PTS^{NIF}-KdpDE-KdpFABC pathway contributes to low potassium stress adaptation and competitive nodulation of *Sinorhizobium fredii*. *mBio*, **13**, e03721-21.